

RESEARCH ARTICLE

10.1002/2016JC011857

Special Section:

Dense water formations in the North Western Mediterranean: from the physical forcings to the biogeochemical consequences

Key Points:

- Continuous monitoring of five consecutive winters of deep convection that reached the seabed, found at a depth of 2300 m
- Observation of the overlapping of the deep convection phases (vertical mixing/restratification; spreading/preconditioning)
- Formation of warmer and saltier new deep water mass “vintages” after each event of deep convection

Correspondence to:

L. Houpert,
loic@lhoupert.fr

Citation:

Houpert, L., et al. (2016), Observations of open-ocean deep convection in the northwestern Mediterranean Sea: Seasonal and interannual variability of mixing and deep water masses for the 2007–2013 Period, *J. Geophys. Res. Oceans*, 121, 8139–8171, doi:10.1002/2016JC011857.

Received 3 APR 2016

Accepted 10 OCT 2016

Accepted article online 13 OCT 2016

Published online 10 NOV 2016

Observations of open-ocean deep convection in the northwestern Mediterranean Sea: Seasonal and interannual variability of mixing and deep water masses for the 2007–2013 Period

L. Houpert¹, X. Durrieu de Madron², P. Testor³, A. Bosse³, F. D’Ortenzio⁴, M. N. Bouin⁵, D. Dausse³, H. Le Goff³, S. Kunesch², M. Labaste³, L. Coppola⁴, L. Mortier³, and P. Raimbault⁶

¹SAMS, Scottish Marine Institute, Oban, Argyll, UK, ²CEFREM, CNRS-UPVD, UMR 5110, Perpignan, France, ³Sorbonne Universités, UPMC, Université Paris 06, CNRS, IRD, MNHN, UMR 7159, Laboratoire d’Océanographie et de Climatologie, IPSL, Paris, France, ⁴Sorbonne Universités, UPMC, Université Paris 06, CNRS, Laboratoire d’Océanographie de Villefranche, Villefranche-sur-Mer, France, ⁵CNRM UMR 3589, Météo-France/CNRS, Toulouse and Univ. Brest, CNRS, IRD, Ifremer, LOPS, IUEM, Brest, France, ⁶Aix Marseille Université, Université Toulon, CNRS, IRD, Mediterranean Institute of Oceanography, UM 110, Marseille, France

Abstract We present here a unique oceanographic and meteorological data set focus on the deep convection processes. Our results are essentially based on in situ data (mooring, research vessel, glider, and profiling float) collected from a multiplatform and integrated monitoring system (MOOSE: Mediterranean Ocean Observing System on Environment), which monitored continuously the northwestern Mediterranean Sea since 2007, and in particular high-frequency potential temperature, salinity, and current measurements from the mooring LION located within the convection region. From 2009 to 2013, the mixed layer depth reaches the seabed, at a depth of 2330m, in February. Then, the violent vertical mixing of the whole water column lasts between 9 and 12 days setting up the characteristics of the newly formed deep water. Each deep convection winter formed a new warmer and saltier “vintage” of deep water. These sudden inputs of salt and heat in the deep ocean are responsible for trends in salinity ($3.3 \pm 0.2 \times 10^{-3}$ /yr) and potential temperature ($3.2 \pm 0.5 \times 10^{-3}$ C/yr) observed from 2009 to 2013 for the 600–2300 m layer. For the first time, the overlapping of the three “phases” of deep convection can be observed, with secondary vertical mixing events (2–4 days) after the beginning of the restratification phase, and the restratification/spreading phase still active at the beginning of the following deep convection event.

1. Introduction

Open-ocean deep convection is a key process that transfers the heat and salt content of the surface layer to the deep ocean and only takes place in a few regions of the world’s oceans. In addition to polar regions such as the Labrador [Lazier, 1973; Clarke and Gascard, 1983], the Greenland [Schott et al., 1993], the Weddell and Ross Seas [Killworth, 1983], open-ocean deep convection can occur in midlatitude regions such as the East/Japan Sea [Kim et al., 2008], and the Mediterranean Sea (Gulf of Lions, Adriatic Sea, Aegean Sea) [CIESM, 2009]. In the Gulf of Lions area (northwestern Mediterranean), a basin-scale cyclonic circulation drives a doming of isopycnals, which helps of the deepening of the mixed layer during intense surface buoyancy loss associated with intense and dry northerly winds (Mistral, Tramontane). The doming of the isopycnals due to the cyclonic gyre and the high surface buoyancy loss can lead to deep mixing and to the formation of the Western Mediterranean Deep Waters (WMDW). The pioneer experiment dedicated to the study of open-ocean deep convection in the Gulf of Lions identified three phases of convection (the preconditioning phase, the intense vertical mixing phase, and the restratification phase with the spreading of the newly formed deep water) [MEDOC Group, 1970]. Recently, several studies illustrate the role of deep convection on transfers of biogeochemical components to the deep water such as oxygen and inorganic and organic matter, contributing to the ventilation and the “feeding” of the deep pelagic and benthic ecosystems [Stabholz et al., 2013; Tamburini et al., 2013]. The deep vertical mixing also impacts the upper ocean through the supply of nutrients from the deep ocean to the euphotic layer [Severin et al., 2014], and is a control parameter of the phytoplankton phenology [Lavigne et al., 2013].

The significant interannual variability of the convective activity in the Gulf of Lions [Mertens and Schott, 1998; L'Hévéder et al., 2013] leads also to an interannual variability of thermohaline characteristics of the WMDW. The evolution of the WMDW thermohaline characteristics formed by deep convection could explain the long-term warming and salting trends observed in the deep layers of the Western Mediterranean (WMED) by several authors [Bethoux et al., 1990, 1998; Leaman and Schott, 1991; Rohling and Bryden, 1992; Krahnmann and Schott, 1998; Rixen et al., 2005; Vargas-Yanez et al., 2010a, 2010b]. The storage of heat, salt, and other properties in the deep layers and their distribution over time and space are of crucial importance for the evolution of this physical-biogeochemical coupled system over the long-term. It is crucial to understand and correctly model this phenomenon in the context of climate change studies.

The deep convection phenomenon is very variable as illustrated by the abrupt changes in WMDW characteristics and stratification, referred as the Western Mediterranean Transition [CIESM, 2009], which occurred during winters 2004–2005 and 2005–2006 [López-Jurado et al., 2005; Schroeder et al., 2006, 2008a; Font et al., 2007; Smith et al., 2008; Zunino et al., 2012]. These changes were related to intense deep water formation events that occurred in the Gulf of Lions region and in the Ligurian subbasin. Moreover, different studies highlight that dense shelf water formation and cascading through the canyons of the Gulf of Lions and Catalan margin can be sometimes important in changing the WMDW stratification and the bottom water mass characteristics, and especially in 2005 [Salat et al., 2006; Canals et al., 2006; Durrieu de Madron et al., 2013; Puig et al., 2013b].

Three causes for such intense deep convection events were identified. First, winter 2004–2005 was one of the coldest and driest winters of the last 40 years [López-Jurado et al., 2005]. Second, Gasparini et al. [2005] showed the appearance of a θ - S anomaly in the Eastern Mediterranean Deep Waters (EMDW) flowing westward through the Sicily channel to the deep Tyrrhenian subbasin, linked to remarkable injection of heat and salt due to the Eastern Mediterranean Transient (EMT) [Klein et al., 1999; Lascaratos et al., 1999; Malanotte-Rizzoli et al., 1999]. The propagation of this θ - S increase from the Eastern Mediterranean could have induced a warming and salting of the intermediate layers of the northwestern Mediterranean [Schroeder et al., 2010]. Modeling studies [Herrmann et al., 2010] moderate the role of the EMT: a high volume of newly formed waters in 2005 but a number of weak deep convection events before winter 2005 could have been effective in inducing a more pronounced Levantine Intermediate Water (LIW) layer, as well as enhanced heat and salt content at intermediate depths. Grignon et al., [2010] suggested that even a normal winter would have led to an intense deep convection in 2004/2005 due to a low pre-winter stratification. Moreover, the high interannual and decadal variability of the potential temperature (θ) and the salinity (S) of Atlantic surface water in the Gulf of Lions [Vargas-Yanez et al., 2010b] can also influence the intensity of deep convection in these years [Rixen et al., 2005].

The intense winter mixing of 2005 is just an example of the deep convection variability. Different observational and modeling works on Open-Ocean Deep Convection were conducted since the 1970s [see Marshall and Schott, 1999 for a review], and the main drivers of the deep convection variability are not yet well defined. Part of it can be explained by the absence of long-term observatory system, and by the fact that we do not know enough the role of the processes involved, particularly at the small scales, which need to be accurately represented in modeling studies. In this article, we will address some of the open questions related to the variability of the deep ocean convection: What are the spatiotemporal scales associated with deep convection? How varies deep convection on an interannual basis? Are the increasing trends in potential temperature and salinity of the WMDW related to deep convection?

We present the recent results on deep convection observed from 7 years (2007–2013) of hydrological and hydrodynamical measurements of the LION mooring line, the MF-LION meteorological buoy and Conductivity-Temperature-Depth (CTD) data collected from research cruises, gliders, and profiling floats (section 2). The methods used to estimate the mixed layer depth, and the heat, salt, and buoyancy contents are presented in section 3. The results mainly derived from observations at the LION mooring line are described in section 4.

Among the 6 years of data available, the November 2009 to December 2010 period is described in detail in section 4.1. During this period, observations provided an invaluable description of the three overlapping, but dominating successively, phases of this representative case of deep convection. In this section, we highlight the variability of the mixed layer which can go from 150 to 2300 m in a couple of months, the intense vertical mixing events and the changes in the θ - S characteristics of the water column.

The temporal and spatial characteristics of the different winters from 2008 to 2013 are presented in section 4.2. In addition, to present the temporal and spatial scales, we also discuss their similarities/differences and assess the role of atmospheric forcing and water column stratification on the triggering of deep convection.

The strong buoyancy losses and the mixing of the water column directly impact the thermohaline characteristics of the newly formed deep water. In section 4.3, we discuss the 6 year evolution of their θ - S properties, together with the temporal scales associated with the evolution of the heat, salt, and buoyancy contents during the different phases of the deep convection are presented in section 4.3. Mooring data and CTD profiles from summer cruise clearly indicate how the successive events of deep convection produce different “vintages” of WMDW, inducing a warming and a salt increase of the deep (1000–2300 m) northwestern Mediterranean.

2. Data

2.1. LION Mooring Line

A multiplatform and integrated monitoring system was setup in the framework of the Mediterranean Ocean Observing System for the Environment (MOOSE, <http://www.moose-network.fr>) to continuously monitor the deep water formation processes in the Gulf of Lions since 2007. Due to the important role of deep convection on climate and ecosystems, this observing system constitutes the multiyear observational system of the international and multidisciplinary programs HyMeX (Hydrological cycle in the Mediterranean Experiment) [Drobinski *et al.*, 2014] and MERMeX (Marine Ecosystem Response in the Mediterranean Experiment) [MERMEX Group, 2011]. MOOSE combines Eulerian observatories and autonomous mobile platforms (gliders, profiling floats): (1) to observe the long-term physical and biological evolution of the NW Mediterranean Sea in the context of the climate change and anthropogenic pollution (metals, oil, hormones, organic compounds, plastics); (2) to detect and identify long-term environmental anomalies; and (3) to build efficient indicators of the status of the pelagic planktonic ecosystem in the Northwestern Mediterranean.

The LION mooring [Testor *et al.*, 2016] is located in the center of the convection zone at 42.03°N, 4.68°E (Figure 1) where the seabed is found at a depth of 2300m. The mooring position is about where the center of the deep convection area is supposed to be [MEDOC Group, 1970; Leaman and Schott, 1991; THETIS Group, 1994]. There were seven deployments (we refer in the following as LIONX to indicate each deployment, where X, from 1 to 7, indicates the different deployment) during which the line was gradually equipped between September 2007 and July 2013 with initially 8 and finally up to 26 instruments. The evolution of the instrumented line over the years is presented in Table 1. Details about the instruments (sampling, data gap) and the calibration are given in Appendix A.

2.2. Météo-France Meteorological Buoy Data

The Météo-France meteorological buoy MF-LION, located at 42.06°N 4.65°E (i.e., 4–4.5 km from the deep mooring location) provides atmospheric observations of surface pressure, wind, air temperature, humidity, radiative fluxes, and sea surface temperature and salinity. In addition, a 250 m instrumented line was installed below the surface buoy since November 2009 and is currently equipped with 20 temperature sensors between 5 and 250 m depth below the sea surface. The evolution of the sensors on the line is shown in Table 2. These NKE sensors measure ocean temperature with a precision of 0.1°C, actual depth with a precision of 0.5 m and are calibrated after every recovery and before every release. Two additional SeaBird SBE37 CTDs were installed at 2 m depth since September 2011 and at 120 m depth since January 2013 (Table 2).

2.3. CTD Profile Data

From 2007 to 2013, CTD profiles from research vessels were collected during several oceanographic cruises (DOCONUG2007, DOCONUG2008, 42N5E, MOOSE-GE2010, CASCADE, MOOSE-GE2011, MOOSE-GE2012, DOWEX2012, DEWEX2013, MOOSE-GE2013, and DOWEX2013) that took place in the northwestern Mediterranean. In total, 385 CTD stations were carried out in the Gulf of Lions area (between 41°N/44°N and 3°E/7°E) and more particularly we use 69 CTD casts located at less than 30 km from the LION mooring (Figure 1).

During all the cruises, pressure, temperature, and conductivity were measured with a CTD Sea-Bird SBE 911plus. Water samples were collected and analyzed with a Guildline Autosol salinometer to calibrate the

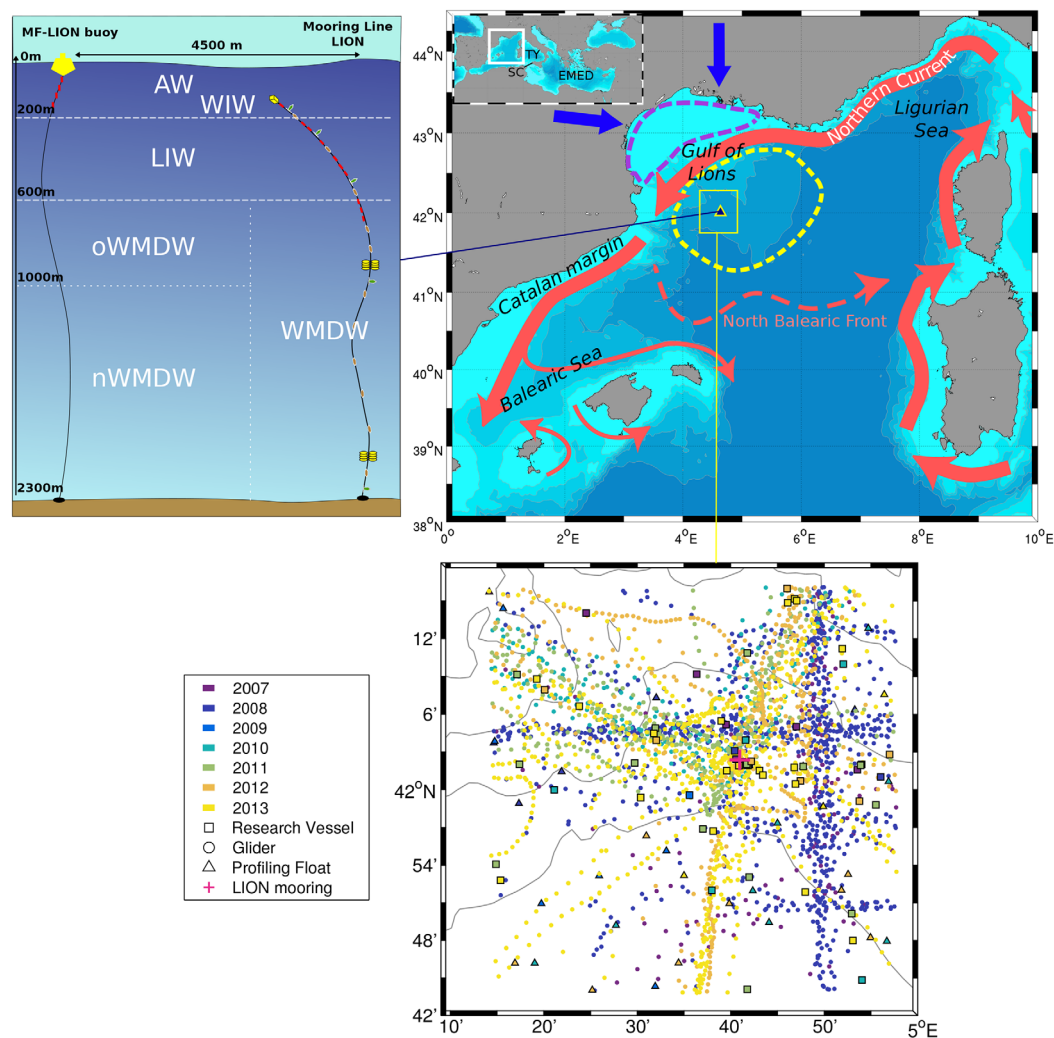


Figure 1. (top left) Mooring designs with the different water masses (AW: Atlantic Water, WIW: Winter Intermediate Water, LIW: Levantine Intermediate Water, (o/n)WMDW: (old/new) Western Mediterranean Deep Water). (top right) Map of the northwestern Mediterranean. (bottom) Map of all the CTD profiles position (research vessel, glider, profiling float) used in this study. (top right) The general circulation patterns are shown in red with the Northern Current flowing along the shelf break from the Ligurian Sea to the Balearic Sea, and the North Balearic Front indicated as an arrow with dashed lines. Prevailing northwestern (Tramontane) and north (Mistral) winds are shown in blue. The dashed yellow line shows the area of Open-Ocean Deep Convection and the purple-dashed line indicates the area of dense water on the shelf. The inset map indicates the different geographic regions described in the manuscript (TY: Tyrrhenian Sea, SC: Sicily channel which separates the Western Mediterranean Sea from the Eastern Mediterranean Sea, EMED).

CTD conductivity sensor. The final accuracy is estimated to be ± 0.004 for salinity and $\pm 0.001^\circ\text{C}$ for potential temperature.

For the period 2007–2013, gliders [Testor *et al.*, 2010] were intensively used in the framework of several European and national projects (see Everyone’s Gliding Observatories (EGO) <http://www.ego-network.org>). Glider profiles were considered as vertical and were checked with quality control procedures defined in the EU FP7 GROOM project. Repeated glider surveys over the Gulf of Lions were conducted between 2007 and 2013, with 38 deployments between January 2007 and August 2013 corresponding to 11,860 profiles (3410 profiles corresponding to 29 deployments were made at less than 30 km around the LION mooring, Figure 1). The calibration of the gliders CTD relies on nearby CTD casts from research vessels and the LION mooring line data (see more details in Bosse *et al.* [2015]).

In addition to the shipborne and the glider CTD casts, about 2500 Argo profiles were collected during the same period (2007–2013), 32 were in the vicinity of the mooring (Figure 1). We used in this analysis only the data flagged as “good” by the Coriolis Data Center (<http://www.coriolis.eu.org/>).

Table 1. Details of the Instruments Shackled to the LION Mooring Line From 2007 to 2013

Deployment Name	LION1		LION2		LION3		LION4		LION5		LION6		LION7		
Date	9 Sep 2007 27 Mar 2008		28 Mar 2008 21 Sep 2008		24 Sep 2008 5 Apr 2009		27 Oct 2009 23 Jun 2010		23 Jun 2010 12 Jun 2011		13 Jun 2011 25 Jul 2012		25 Jun 2012 17 Jun 2013		
Temperature Sensor	Type	RBR		RBR		RBR		RBR		RBR		Seabird		Seabird	
		TR-1060		TR-1050/1060		TR-1050/1060		TR-1050/1060		TR-1050/1060		SBE56		SBE56	
	Nominal depth (m)	250–350–500–600		150–200–230–250–350–400–450–550–600–650		150–200–230–250–350–400–450–550–600–650		150–200–230–250–350–400–450–550–600–650		150–200–230–250–350–400–450–550–600–650		150–200–230–250–350–400–450–550–600–650		150–200–230–250–350–400–450–550–600–650	
	Sampling	15 s		15 s		15 s		15 s		15 s		15 s		15 s	
Conductivity-Temperature	Type	Seabird SBE37SM		Seabird SBE37SM		Seabird SBE37SM		Seabird SBE37SM		Seabird SBE37SM		Seabird SBE37SM		Seabird SBE37SM	
	Nominal depth (m)	170–700–1500–2300		170–300–500–700–1500–2300		170–300–500–700–850–1100–1300–1500–1750–2000–2300		170–300–500–700–850–1100–1300–1500–1750–2000–2300		170–300–500–700–850–1100–1300–1500–1750–2000–2300		170–300–500–700–850–1100–1300–1500–1750–2000–2300		170–300–500–700–850–1100–1300–1500–1750–2000–2300	
	Sampling	6 min		6 min		3 min/6 min		3 min/6 min		3 min/6 min		3 min/6 min		3 min/6 min	
Current meter	Type	Aanderaa RCM9	RDI ADCP	Aanderaa RCM9	RDI ADCP	Nortek Aquadopp	Nortek Aquadopp	Nortek Aquadopp	Nortek Aquadopp	Nortek Aquadopp	Nortek Aquadopp	Nortek Aquadopp	Nortek Aquadopp	Nortek Aquadopp	
	Nominal depth (m)	1000	2300	1000	2300	150–250–500–1000	150–250–500–1000–2300	150–250–500–1000–2300	150–250–500–1000–2300	150–250–500–1000–2300	150–250–500–1000–2300	150–250–500–1000–2300	150–250–500–1000–2300	150–250–500–1000–2300	
	Sampling	30 min	30 min	30 min	30 min	30 min	30 min	30 min	30 min	30 min	30 min	30 min	30 min	30 min	

2.4. Miscellaneous Data (ERA-Interim Atmospheric Reanalysis, Ocean Color Images)

2.4.1. ERA-Interim Reanalysis

In this study, we are interested to discuss the daily evolution of the mixed layer depth compared to the surface buoyancy and heat losses. In addition, we also want a flux-product to compare different winters with each other. We choose to use the ERA-Interim reanalysis essentially because of these two aspects: the chronology of the flux at a daily scale and the long-term temporal homogeneity [Herrmann et al., 2011]. Moreover, the four components of the net heat flux are calculated in a consistent way, at the same time.

Based on the European Centre for Medium-Range Weather Forecasts (ECMWF) numerical weather prediction model, the ERA-Interim reanalysis data set contains consistent atmosphere and sea surface analyses for the period starting in 1979 [Dee et al, 2011]. The reanalysis makes use of the ECMWF Integrated Forecast System at T255 spectral resolution (80 km horizontal resolution) with 91 vertical levels. We considered here the daily fields of the air-sea fluxes (downward and upward short-wave radiation, downward and upward long-wave radiation, latent heat flux, sensible heat flux, total precipitation, and evaporation) in order to compute the daily net heat flux (Q_{net}) and the net freshwater flux out of the ocean.

2.4.2. Ocean Color Images

The 8 day Level 3 standard mapped images of MODIS Aqua surface chlorophyll concentration at 4 km resolution were obtained from the NASA web site (<http://oceancolor.gsfc.nasa.gov/>) for the 2007–2013 period.

3. Methods

3.1. Estimation of the Mixed Layer Depth

Since the buoy oceanographic sensors and the deep mooring instruments are not the same, the resolution and the accuracy of the different sensors are also different (see Tables 1 and 2). Initially, observations of the deep

Table 2. Details of the Instrument Mounted on the MF-LION Surface Buoy From 2009 to 2013

Date	13 Nov 2009 2 Mar 2010	2 Mar 2010 5 Nov 2010	5 Nov 2010 17 Jun 2013
NKE SP2T Temperature Sensor	Nominal depth (m) 10–20–50–100–200		10–200
	Sampling 5 min		5 min
SBE37 Seabird CTD	Nominal depth (m) n.a.		n.a.
	Sampling n.a.		n.a.

Table 3. Criterion Used to Calculate the Mixed Layer Depth at the LION Site

	2007–2009 (No Temperature Data in the First 150 m, Except SST)	2009–2013 (Temperature Sensors Between 1 and 200 m)
MLD < 300 m	$\Delta\theta_1 = 0.6^\circ\text{C}$, reference level: 1 m	$\Delta\theta_1 = 0.1^\circ\text{C}$, reference level: 10 m
MLD \geq 300 m.	$\Delta\theta_2 = 0.01^\circ\text{C}$, reference level: 300 m	

mooring line and the buoy sensors are merged, and a linear interpolation in time and along the vertical coordinate results in potential temperature profiles gridded on 1 m bins, every 30 min. Because of the different accuracy of the sensors in the upper and in the deep parts of the water column and the weak deep stratification (from a depth of 1000 m to the bottom), we adopt a double criterion to estimate the mixed layer depth.

The Mixed Layer Depth (MLD) is calculated for the first 300 m of the upper water column using a potential temperature criterion $\Delta\theta_1 = 0.1^\circ\text{C}$ and a reference level at 10 m. If the MLD calculated with the $\Delta\theta_1$ criterion is deeper than 300 m, we used a second criterion $\Delta\theta_2 = 0.01^\circ\text{C}$ and a reference level at 300 m to define the MLD. This second criterion is required to define a more accurate MLD, as potential temperature gradients at the base of the ML can be smaller than $d\theta_1 = 0.1^\circ\text{C}$ in winter when the mixing exceed 1000 m depth (see Appendix B for details).

There was no instrument below the MF-LION surface buoy before November 2009, only the sea surface temperature sensor at 1 m depth could be used in the MLD calculation. Due to the low accuracy of this sensor, we had to calculate the MLD in the first 300 m using a criterion $\Delta\theta_1 = 0.6^\circ\text{C}$ and a reference level at 1 m. If the MLD is deeper than 300 m, we used as for the 2009–2013 period, a secondary criterion $\Delta\theta_2 = 0.01^\circ\text{C}$ and a reference level at 300 m depth to calculate the MLD below 300 m depth (Table 3; Appendix B for more details).

3.2. Estimation of the Heat and Salt Contents of the Water Column

The vertical resolution of CTD measurements below the MF-LION buoy and along the LION mooring line enables heat or salt budget calculations for specific water masses. Merging data from both sources, there are 5–17 additional potential temperature levels in the first 150 m since 2009 and two additional salinity levels (at 2 m depth since 2011 and 120 m depth since 2013), compared to the number of sensor levels on the LION mooring line alone.

Observation levels have been distributed throughout the water column to reflect an optimized sampling along the vertical of climatological profiles. Since 2009 with 20 potential temperature levels and 10 salinity levels, distances between potential temperature levels are about 50 m in the upper 700 m of the water column and about 250 m deeper down. Distances between salinity levels are about 250 m throughout the water column. Before budget calculations, we performed a linear interpolation of potential temperature and salinity versus depth to obtain 1 m resolution profiles from the surface (2 m) to the seabed (2300 m) every 30 min.

To quantify the error in heat or salt budget in a specific layer due to this linear interpolation, we use a reference database created from 1 m-binned CTD profiles (from research vessels, gliders, and profiling floats) carried out in a 30 km radius (typical scale of the mesoscale processes in summer in the deep convection area) centered on the mooring.

We estimate the error due to the vertical interpolation, for each different configuration of the deep mooring and surface buoy arrays (shown in section 4.3.1). By taking into account the data availability of the merged mooring-buoy line, we get 33 different configurations between September 2007 and July 2013 for the daily data. For each layer and for each time step (daily), a reference profile is chosen as the most stratified profile in a specific time window (2 months for the 1–200 m, 200–600 m, and the 600–1000 m layers; 6 months for the deepest layers: 600–2300 m and 1000–2300 m). If there is no profile available during this time window, we choose the most stratified profile from a climatology created from the 6 years of data, using the same time window but on climatological month. We calculate the error in potential temperature, salinity, and potential density as the difference between the high-resolution profile and the same profile subsampled at the mooring vertical resolution and linearly interpolated.

3.3. Estimation of the Integrated Buoyancy Content of the Water Column

The influence of the water column stratification on the deep convection occurrence can be explored using a 1-D approach, where only the surface buoyancy flux drives overturning and deepens the mixed layer (i.e., when the surface buoyancy flux is positive, buoyancy is removed from the ocean, the water gets denser, and deepening of the mixed layer convection arises). *Grignon et al.* [2010] and *L'Hévéder et al.* [2013] used this approach in the northwestern Mediterranean Sea. *Lilly et al.*, [1999] followed the same assumptions to study the mixed layer property evolution in a θ - S space in the Labrador Sea.

In our study, this 1-D approach is used during the period going from the end of the preconditioning period (November) to the beginning of the restratification (corresponding in our case to end of February). At that time of the year, the mooring area is dominated by vertical mixing and away from the boundary circulation where the horizontal currents are known to be intense and mostly oriented along the bathymetry (f/H contours). Thus, the main lateral contribution is due to eddies. Following a method described in *Lilly and Rhines* [2002] and *Lilly et al.* [2003] to detect eddies from mooring currents time series, *Houpert* [2013] detected more than 30 eddies between October 2009 and July 2012. Over this whole time period, eddies are present about 10% of the time at the mooring. Some of those eddies could have been identified as Submesoscale Coherent Vortices (SCVs) described by *McWilliams* [1985]. These SCVs induce the propagation of columnar buoyancy perturbations typically of 0.05 – $0.15 \text{ m}^2 \cdot \text{s}^{-2}$ as discussed in *Bosse et al.* [2016]. The eddy-induced buoyancy flux would then represent about 0.5–1.4% of the total integrated buoyancy flux over the winter (typically $1.15 \text{ m}^2 \cdot \text{s}^{-2}$). Therefore, eddy lateral buoyancy fluxes can be considered, at the first order, as negligible effect on the buoyancy content budget of the deep convection zone.

In this work, we will further examine into details IS(1000) the columnar buoyancy of the first 1000 m and compare it to the integrated surface buoyancy losses from 1 November to the end of February. The methodology used to calculate this stratification index is detailed in Appendix C.

4. Results and Discussion

4.1. Water Column Variability and Transients in the Deep Convection Area in 2009/2010

Among the 6 year time series available, a specific focus on the November 2009 to July 2010 period is made. For the first time, the MF-LION surface buoy was equipped with subsurface temperature sensors. The LION mooring was fully instrumented and for the first time monitored the preconditioning, the intense vertical mixing, and the spreading/restratification phases. As for the winters of deep convection (2009, 2011, 2012, 2013), intense deep vertical mixing is observed during winter 2010, as revealed by the complete homogenization of the water column during the month of February 2010 (Figures 2a–2c), and the strong vertical currents (Figure 3c).

4.1.1. Evolution of the θ - S Characteristics of the Mixed Layer and the Water Column During a Deep Convection Event

4.1.1.1. The Deepening of the Mixed Layer

In September, the monthly net heat flux is close to $0 \text{ W} \cdot \text{m}^{-2}$. The strong heat loss starts to increase later in October and November. The negative heat fluxes (Figure 3d) result in gradually cooling surface layers (Figure 2a), and in mid-December the first 200 m of the water column is fully mixed (Figure 2a), indicating a mixed layer reaching 200 m. At the end of December and beginning of January, the upper sensor (at 170 m, dark blue line in Figures 2b and 2c) records a potential temperature (salinity) dropping rapidly to 13.05°C (38.4). This different water mass can be seen more clearly on a θ - S diagram, where it has a very distinct signature, colder, and fresher (Figure 4b1), compared to the “classical” Atlantic Water (AW) that can be found usually in this area in the surface layer (Figure 4a1). The arrival of this new water mass corresponds to an increase in the horizontal velocities, with intensification in the upper part of the water column (see current meter at 250 m in Figure 3b). This could be the signature of mode waters, the Winter Intermediate Water (WIW) [*Millot*, 1999] formed around the mixed patch and being advected into the deep convection area, where the surface waters are usually saltier.

After this first period of strong cooling (drop of $\approx 0.3^\circ\text{C}$ at 170 m), the mixing goes deeper with strong vertical currents detected at 250 m ($\approx 15 \text{ cm} \cdot \text{s}^{-1}$) and 500 m depth ($\approx 5 \text{ cm} \cdot \text{s}^{-1}$) from 9 to 12 January (Figure 3c), associated with strong daily heat losses ($\sim -800 \text{ W} \cdot \text{m}^{-2}$, Figure 3d). The warm and salty LIW is therefore entrained by the vertical mixing, resulting in a decrease in potential temperature and salinity at 300 and 500 m depths (see blue and cyan lines in Figures 2b and 2c). At the same time, the heat and salt content of

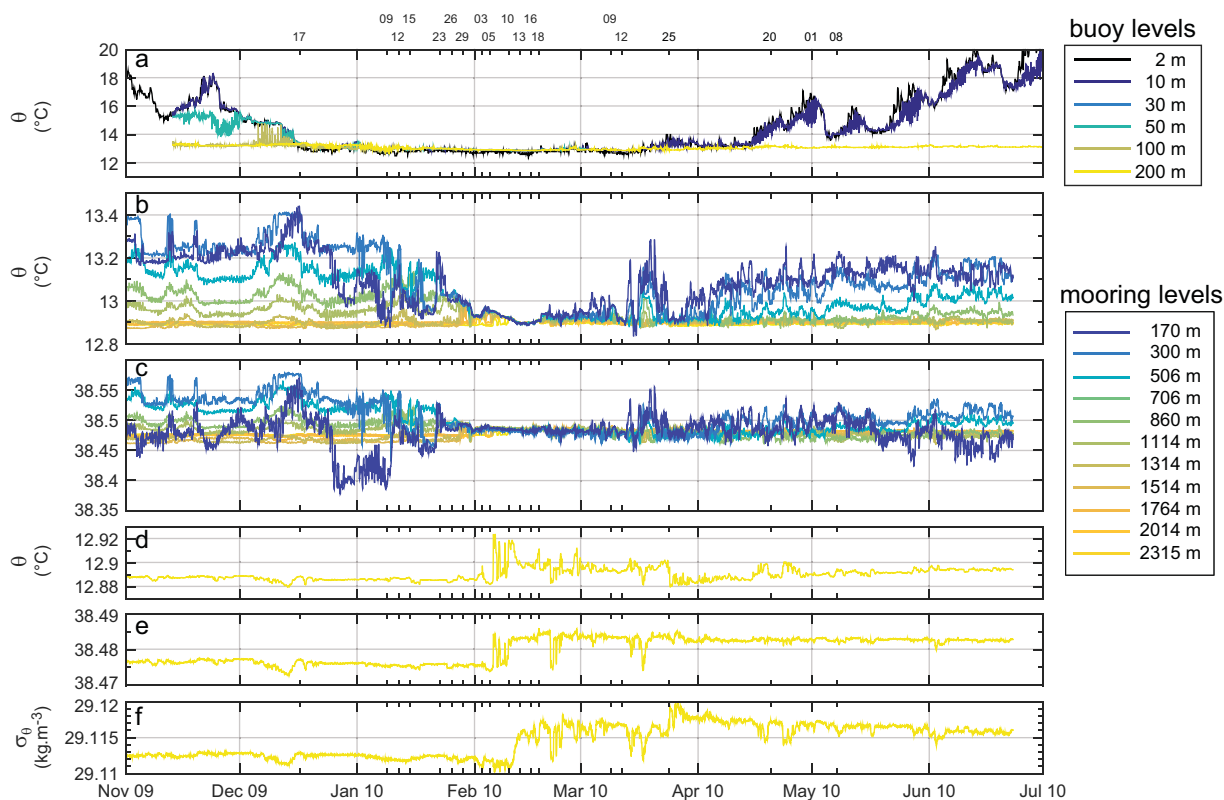


Figure 2. (a) Bihourly potential temperature from the sensors mounted below the surface buoy LION (from 2 to 200 m), (b) potential temperature, and (c) salinity recorded by Seabird Microcats from 170 to 2330 m between November 2009 and July 2010. The near-bottom potential (d) temperature, (e) salinity, and (f) potential density anomaly are also presented with a separate vertical scale.

the LIW is vertically homogenized within the surface layer and this induces an increase of potential temperature and salinity in the mixed layer above (Figures 2a and 2b, dark blue line).

From 15 to 23 January, the atmospheric forcing and the vertical mixing weaken with less intense vertical velocities (Figure 3c) and potential density in the upper ocean layer stops increasing (Figure 3a). Between 23 and 26 January, a sharp increase in potential temperature (0.2°C) and salinity (0.1) at 170 m depth indicates the entrainment of LIW in the mixed layer. At that time, the MLD reaches 800 m (Figure 3e). The deepening of the mixed layer, not related to a parallel increase of the vertical velocity, could indicate that this signal corresponds to the advection of a homogeneous water column in the area rather than a local formation in a 1-D framework.

From 27 to 29 January, the mixed layer deepens more than 500 m. The event is associated with an increase in surface heat loss and vertical velocities (more than $5\text{ cm}\cdot\text{s}^{-1}$ at 250, 500, and 1000 m depth). The vertical mixing increases until the MLD reaches 2000 m on 1 February (Figure 3e). Vertical mixing stops for a couple of days on 3 February, at the same time that atmospheric heat loss decreases (Figures 3c and 3d). However on 5 February, an important increase in potential temperature (0.04°C) and salinity (0.01) is recorded at 2300 m depth (Figures 2d and 2e), which indicates that the mixed layer, saltier and warmer than the deep waters, reaches the seabed. At that time, the potential density of the bottom water is still the same $29.111\text{ kg}\cdot\text{m}^{-3}$ (Figure 2f). When the mixed layer reaches the deep layer, the colder and fresher deep waters associated with old WMDW (Figures 4a2 and 4b2) are transformed, through this heat and salt input coming from the mixed layer, into a new water mass (Figure 4c2). At that time, no sign of violent mixing at great depths can be found, as shown by weak vertical velocities measured at 1000 m depth (Figure 3c).

4.1.1.2. Deep Convection Down to the Bottom

On 10 February very strong heat losses (daily values exceed $-600\text{ W}\cdot\text{m}^{-2}$) induce violent vertical mixing, with the strongest vertical currents recorded during this winter at 250, 500, and 1000 m depth (Figures 3c and 3d). Vertical speeds sporadically exceed $+10$ and $-15\text{ cm}\cdot\text{s}^{-1}$.

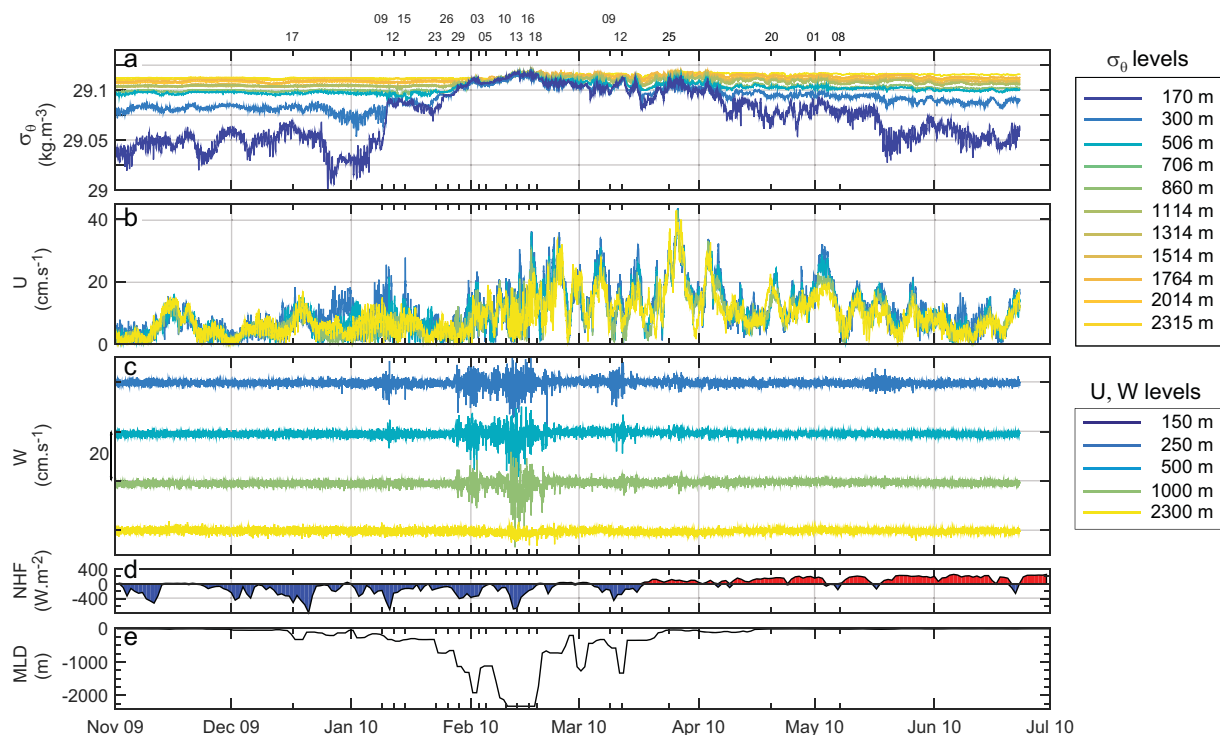


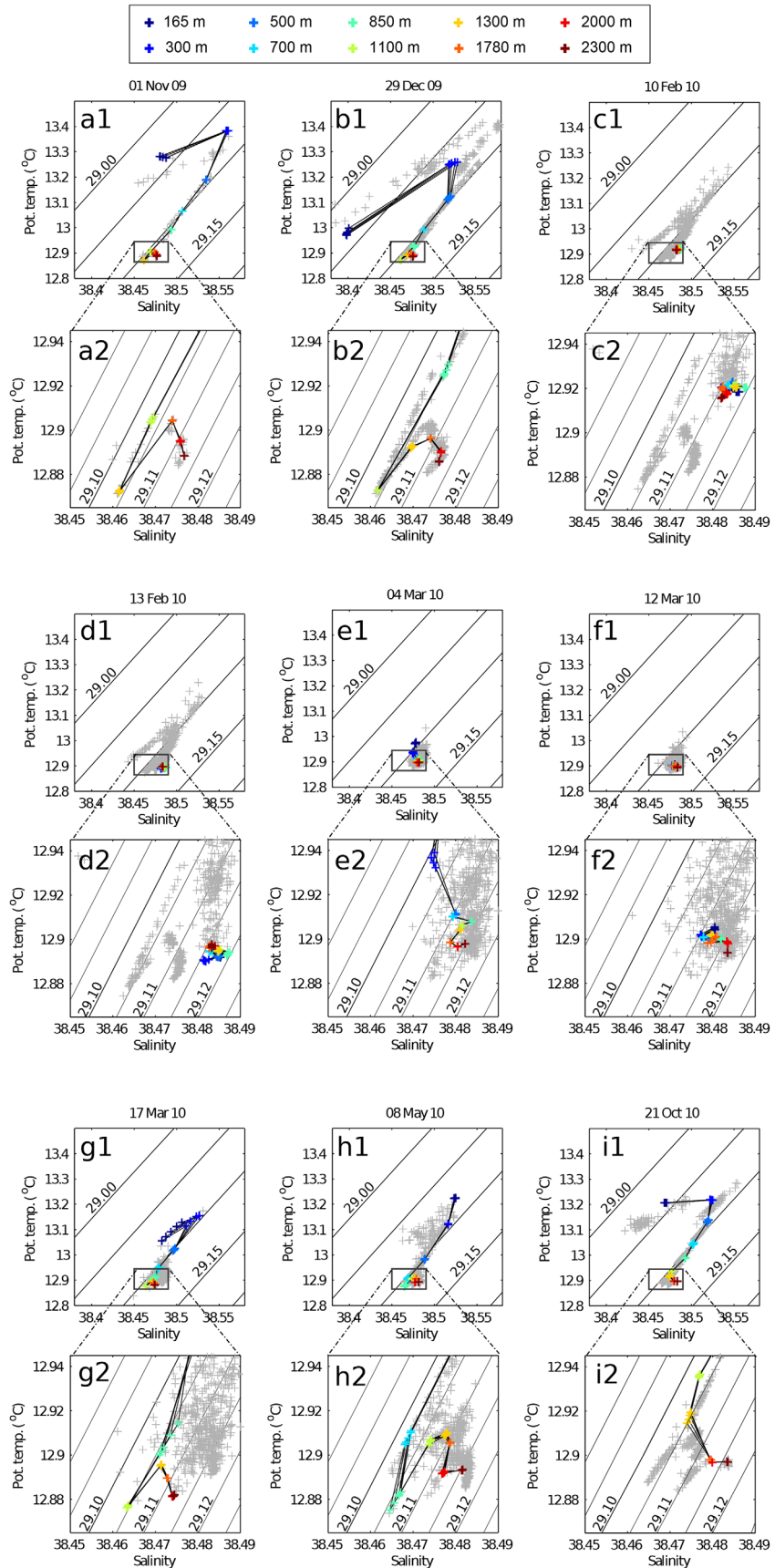
Figure 3. Bihourly potential density (a) recorded by Seabird Microcats from 170 to 2330 m between November 2009 and July 2010, with (b) horizontal and (c) vertical currents recorded at 250, 500, 1000, and 2330 m, (vertical currents are offset by $20 \text{ cm}\cdot\text{s}^{-1}$), (d) daily surface net heat flux estimated by ERA-Interim at the mooring location, and (e) mixed layer depth estimated from the mooring data (see section 3.1 in the manuscript for a description of the chosen criterion).

From 10 to 13 February, the potential temperature of the whole water column decreases by more than 0.02° (Figures 2d, 4c2, and 4d2), due to the strong heat losses and to the fact that the deepening of the mixed layer is constrained by the seafloor. During the same period, the salinity does not present any detectable change. The winter buoyancy fluxes are largely dominated by the heat fluxes [Grignon *et al.*, 2010], so the salinity of the newly formed deep water is mostly set by the salt content of the water column before the deep convection, while its potential temperature results from a combination of the initial heat content of the water column and of the surface heat fluxes.

On 16 February, one day after the end of the violent vertical mixing phase, horizontal currents increase, reaching $30\text{--}38 \text{ cm}\cdot\text{s}^{-1}$ between 170 and 1000 m deep and $20 \text{ cm}\cdot\text{s}^{-1}$ at 2300 m (Figure 3b). This increase of the horizontal velocities occurs after the water column reached its highest density level of the whole year (Figure 3a), and can be seen as an adjustment of the ocean: once the atmospheric forcing stopped, the potential energy gained by the water column during the whole vertical mixing period is converted into kinetic energy.

4.1.1.3. End of the Deep Convection and Horizontal Homogenization

After the last event of strong vertical mixing (12 March), the water column stratification progressively increases (Figure 3a). Thanks to surface heat gain (Figure 3d) and advection of light waters near the surface [Leaman and Schott, 1991; Schott *et al.*, 1996; Herrmann *et al.*, 2008], vertical gradients of potential temperature, salinity, and density increase inside the water column. Potential temperature difference between the surface and 200 m depth starts to be higher than 1°C on 20 April (Figure 2a). First May, the potential temperature difference between the surface and 200 m depth reaches 3°C (Figure 2a). From mid-April to the end of May, the potential temperature stratification in the upper 200 m fluctuates between 0.005 and $0.015^\circ\text{C}\cdot\text{m}^{-1}$ (Figure 2a). The scale of variability associated with these changes in the upper ocean stratification (Figure 2a) is typically of 5–10 days and are similar to the scale of variability observed in the horizontal velocities at all levels (Figure 3b). This suggests an important role of submesoscale and mesoscale circulation features such as eddies during the restratification phase [Houpert 2013; Bosse *et al.*, 2016]. Similar eddies were also observed in other places such as the Labrador Sea [Lilly and Rhines 2002; Lilly *et al.*, 2003;



Hátún *et al.*, 2007; De Jong *et al.*, 2014] or the Irminger Sea [Fan *et al.*, 2013], where they play an important role in the restratification of the deep convection area.

The Levantine Intermediate Water (between 200 and 500 m deep) is easily distinguishable in the Gulf of Lions, because of its maximum in salinity. On a θ - S diagram, this water mass can be found between a potential density anomaly of 29.05 and 29.10 $\text{kg}\cdot\text{m}^{-3}$, as a maximum salinity and a local maximum in potential temperature (Figure 4a1). The LIW is completely mixed during deep convection events (Figures 4d1, 2b, and 2c), but, as soon as the atmospheric forcing stops (the net heat flux becomes positive), the strong horizontal mixing associated with mesoscale features (Figure 3b), brings back the LIW into the deep convection area, such as on 17 March (Figure 4g1, 2b, and 2c).

4.1.2. Vertical Mixing and Convective Plumes

The LION mooring offers for the first time a complete year of observation of the deep convection process. The significant vertical velocities observed during the intense vertical mixing phase exceed +10 and $-15 \text{ cm}\cdot\text{s}^{-1}$, and are in agreement with previous observations of convective plumes of horizontal scale of 1 km characterized by downward vertical velocities up to $10 \text{ cm}\cdot\text{s}^{-1}$. These small-scale features were first observed using isobaric floats [Voorhis and Webb, 1970], then using moored ADCPs [Schott and Leaman, 1991; Schott *et al.*, 1996]. More recently, downward vertical velocities up to $10 \text{ cm}\cdot\text{s}^{-1}$ were indirectly inferred using gliders [Merckelbach *et al.*, 2010; Frajka-Williams *et al.*, 2011; Bosse *et al.*, 2014]. These plumes act at short temporal and spatial scales and result in the mixing of the properties over the convection area.

If the spatial (single-point) and temporal (30 min) sampling of the current meters on the mooring is not enough to resolve the convective plumes (diameter of 800–1000 m in the Gulf of Lions) [Marshall and Schott 1999], the θ - S sensors of the mooring seem to give us some clues about the presence of convective plumes which may have decelerated and do not have vertical velocities anymore. This detection is possible particularly at the beginning of the intense vertical mixing phase, when the area is not completely mixed, and the old deep water can still be distinguished from the newly formed deep waters. On 7 February and 8 February, two isolated peaks in potential temperature and salinity can be distinguished at 2300 m (Figures 2d and 2e). The length of these peaks is, respectively, 12 h and 6 h, while the mean horizontal velocities associated with these events are, respectively, 6 and $14 \text{ cm}\cdot\text{s}^{-1}$, without associated vertical velocities. These high-frequency events seen in the potential temperature and salinity bihourly time series (Figures 2d and 2e) are certainly related to the presence of small-scale plumes, already observed in Greenland Sea [Schott *et al.*, 1993] and in the Gulf of Lions [Schott and Leaman, 1991; Schott *et al.*, 1996], which act as a mixing agent [Send and Marshall, 1995; Marshall and Schott 1999]. Since in these cases there is not vertical mixing synchronous with the appearance of these θ - S anomalies, the structures detected are not “active” in the vertical mixing. In addition to their important role in diapycnal mixing, these small-scale structures play certainly an important role in the homogenization of the mixed patch, through isopycnal mixing. Setting up specific experiments to study the scales and the energy associated with these vertical and horizontal small-scale processes could allow us to better understand how the vertical/diapycnal mixing and the horizontal/isopycnal mixing occur in the deep convection area.

4.1.3. Secondary Event of Deep Vertical Mixing

From 18 February to 8 March, the net heat flux from the atmosphere to the ocean is close to zero and even occasionally positive, and consequently the vertical mixing stopped. High horizontal currents start to advect stratified waters into the mooring area (Figures 3a and 4e). The last strong winter cooling event occurs from 9 to 12 March, associated with an increase in vertical currents down to, at least 1000 m depth, where the deepest current meter showing intense vertical motion is located (Figure 3c). Based on a θ - S diagram, the water column was homogeneous down to about 1750 m depth (Figure 4f).

Restratification processes seem to dominate as soon as the atmospheric forcing stops to trigger active mixing. Strong net surface buoyancy losses can trigger secondary events of deep vertical mixing if they are

Figure 4. θ - S diagrams from all the mooring Microcats (1) with an enlargement on the deep waters (2). The nominal depth of the different instruments is indicated by the color marks (from 170 to 2300 m), while gray marks correspond to the data of the past month. The slanting black lines are σ_θ contours. Particular stages of the evolution of the water column from December 2009 to November 2010 are described: (a–d) the mixed layer deepening; (b) the formation of WIW; (d) the formation of the new WMDW; (e) the overlapping of the restratification phase of the deep layer with (f) a second event of vertical mixing; (g, h) restratification of the LIW and WMDW after the winter mixing associated with mesoscale features; and (i) the new stratification of the deep waters in October 2010 prior to the 2011 deep convection (note the significant changes compared to (a) November 2009, before the 2010 deep convection event).

superior to the buoyancy content of the water column, highlighting the overlapping of the intense vertical mixing phase and the restratification phase.

4.1.4. Role of the Atmospheric Forcing on Setting Up the θ/S Characteristics of the Newly Formed Deep Water

In winters 2004–2005 and 2005–2006, abrupt changes, referred as the Western Mediterranean Transition [CIESM, 2009], were observed in the Western Mediterranean Deep Water characteristics and stratification [López-Jurado *et al.*, 2005; Schroeder *et al.*, 2006, 2008a; Font *et al.*, 2007; Smith *et al.*, 2008; Zunino *et al.*, 2012]. In November 2009, the deep stratification of the water column in the Western Mediterranean still indicates the presence of three distinct deep water masses (Figure 4a2). In this subsection, we will present the effect of the surface net heat flux on the characteristics of the newly formed deep waters during the intense vertical mixing phase of a deep convection event. A detailed analysis of the evolution of the deep waters in the Gulf of Lions from 2007 to 2013 is made in subsection 4.3.3.

The post-2005 newly formed deep waters (nWMDW), which are saltier and denser than the “old” deep waters (pre-2005, oWMDW), are essentially found below 1300 m. Lowermost potential temperature and salinity observed in the 750/1200 m layer (Figures 4a2, 4b2, 4g2, 4h2, and 4i2), correspond to the “old” WMDW θ/S characteristics that can be found in other part of the basin. On 10 February 2010, the potential temperature at 2300 m depth increased by 0.03°C once the mixed layer reaches the seabed (see Figures 2d, 3e, and 4c2). The consecutive 10 days of strong heat loss (Figure 3d) decrease the mixed layer potential temperature by 0.02°C (Figures 2d and 4d2). During this 10 day period, there are no perceptible salinity changes (Figures 2e and 4d2), and the potential density increases by 0.004 kg.m⁻³ (Figures 2f and 4d2). During this period of 10 days of intense vertical mixing, the evaporation does not seem to play a significant role in setting up the characteristics in salinity of the newly formed deep waters.

These observations are in agreement with previous studies which related the characteristics of the newly formed water mass to the frequency and the intensity of the surface forcing [Artale *et al.*, 2002; Grignon, 2009] and to the heat and salt content of the pre-winter oceanic state [Grignon *et al.*, 2010; Herrmann *et al.*, 2010; Schroeder *et al.*, 2010]. Furthermore, the surface heat losses during this 10 day period are very important in setting the potential temperature and density of the newly formed deep water. The heat content of the water column, together with the surface net heat flux, is responsible for the evolution of the potential temperature of the mixed layer during the whole deepening phase. However, once the mixed layer reaches the seabed, the surface net heat losses will be the main driver in the decrease of the mixed layer potential temperature and in setting up the final potential temperature and density of the newly formed deep water.

4.2. Interannual Variability of the Recent Deep Convections Events

We derive and compare here the temporal and spatial characteristics of the various winter convection events. We then further examine the role of atmospheric forcing and water column stratification for six consecutive winters.

4.2.1. Mixed Layer and Multiple Events of Vertical Mixing

Characteristics of five successive winters of open-ocean deep convection (2009–2013) are summarized in the Table 4. The chronology is different according to the events, mainly due to the interannual variability of the heat losses and the stability of the water column (discussed in section 4.2.4). For example, in 2011, the vertical mixing penetrates below the LIW 1 month earlier than in 2009, 2010, 2012, and 2013 (Figure 5). On 26 December 2010, the MLD reaches already 1200 m (Figure 5). The water column is homogenized (decrease in potential temperature and salinity in Figures 6a and 6b and increase in potential density in Figure 7a on the 170, 300, and 700 m-Microcat), while significant vertical velocity superior at 15 cm.s⁻¹ are recorded at 150, 250, and 500 m depth (Figure 7c).

Some common features can be pointed out from the analysis of the five events of deep convection observed between 2009 and 2013. Due to the surface heat and buoyancy losses, the mixed layer starts to deepen in September and reaches the base of the AW (150/200 m deep) generally in December. The time needed for the mixed layer to deepen from the base of the AW down to the bottom is between 1 and 2 months (Table 4). Compared to the other winters, heat losses in the beginning of February 2012 are very strong (the mean net heat flux from 1 to 15 February is about -440 W.m^{-2}) and the MLD deepens by 2000 m (from the LIW to the bottom), reaching the seabed in only 1 week (Figure 5). This deepening of the MLD is associated with important vertical velocities (15 cm.s⁻¹) that vary at high-frequency and are

Table 4. Main Scales Associated With the Different Deep Convection Events From 2008 to 2013

	2008	2009	2010	2011	2012	2013
Mixed layer deepens below 150 m	17 Dec 2007	15 Dec 2008	17 Dec 2009	15 Dec 2010	08 Jan 2012	08 Dec 2012
WIW detected	21 Dec 2007	30 Dec 2008	9 Jan 2010	16 Dec 2010	03 Feb 2012	All the year 2012
($S < 38.42$ at 150 m)						
LIW mixed	02 Apr 2008	08 Jan 2009	23 Jan 2010	19 Dec 2010	07 Feb 2012	25 Jan 2013
Mixed Layer reaches the bottom	No (700 m)	12 Feb 2009	10 Feb 2010	27 Jan 2011	10 Feb 2012	13 Feb 2013
Bottom pot. temperature increase	x	0.040°	0.030°	0.022°	0.042°	0.032°
Bottom salinity increase	x	0.009	0.007	0.006	0.012	0.004
End of vertical mixing (until 1000 m)	x	26 Feb 2009	20 Feb 2010	05 Feb 2011	23 Feb 2012	28 Feb 2013
Pot. temperature decrease of the mixed layer once the bottom is reached	x	0.024°	0.019°	0.012°	0.032°	0.032°
Bottom pot. density increase at the end of the mixing ($\text{kg}\cdot\text{m}^{-3}$)	x	0.0044	0.0062	0.0030	0.0090	0.0030
Max. deepening of mooring head	0	350 m	550 m	550 m	550 m	550 m
Second vertical mixing event						
Time period	x	06 Mar 2009 to 8 Mar 2009	9 Mar 2010 to 12 Mar 2010	1 Mar 2011 to 4 Mar 2011	7 Mar 2012 to 11 Mar 2012	13 Mar 2013 to 17 Mar 2013
Maximal depth detected on current meters	x	>1000 m	>1000 m	>500 m	>1000 m	>1000 m
Maximum of MLD	x	2000 m	1500 m	1700 m	2300 m	1800 m
End of the second vertical mixing period	4 Apr 2008	9 Mar 2009	13 Mar 2010	5 Mar 2011	13 Mar 2012	21 Mar 2013
Area of low surface chl-a ($<0.15 \text{ mg}\cdot\text{m}^{-3}$) in km^2	0	16,350	13,006	15,790	17,863	23,583
Area of low surface chl-a ($<0.25 \text{ mg}\cdot\text{m}^{-3}$) in km^2	1,487	34,162	29,180	24,111	41,616	56,351
New density class of WMDW ($\text{kg}\cdot\text{m}^{-3}$)	None	29.114–29.116	29.116–29.119	None	29.119–29.126	None
Formation rate associated with the new density class (in Sv)		1.14	0.91		1.25	

consistent with past observations of vertical mixing in plumes of horizontal scale of $O(1 \text{ km})$ (order of magnitude of 1 km) carried out by *Voorhis and Webb* [1970], *Schott and Leaman* [1991], and *Schott et al.* [1996]. A more detailed analysis discussing the water column stratification and the surface buoyancy losses for this specific event is made in section 4.2.4.

Once the mixed layer reaches the seabed, a jump in potential temperature (Figure 6d), salinity (Figure 6e), and potential density (Figure 6f) can be observed on the near bottom Microcat data. The timing of the deep vertical mixing can be seen on all the current meters except the deepest one, located 30 m above the seabed in the bottom boundary layer. All the deep convection winters present a common feature with a violent vertical mixing phase of the whole water column lasting between 9 and 12 days, which lead to a potential temperature decrease of the whole water column between 0.015 and 0.03°C (Figure 6d and Table 4). After the MLD reached the bottom, we do not see significant changes in salinity of the deep water during the 10/14 day period of vertical mixing (Figure 6e), which is in agreement with *Grignon et al.* [2010] who show that the haline component of the buoyancy flux is negligible compared to the thermal component. The salinity of the newly formed deep water is therefore mostly set by the salt content of the water column before convection, while the potential temperature of the newly formed deep water results from the combination of the initial heat content and the surface heat fluxes, as discussed for the 2010 winter in section 3.1.4.

All winters from 2009 to 2013 present a secondary vertical mixing period that generally occurs in March after the main convective event, when the restratification of the water column has already begun. This is the first time that these secondary vertical mixing events are observed, thanks to the high temporal resolution monitoring from full water column mooring. These short events (2–4 days) happen when the restratification has already begun. By that time, the water column is weakly stratified and a 3–6 days period of strong heat losses (typical duration of a winter storm) is enough to destabilize the upper water column leading to vertical mixing that can easily reach great depths.

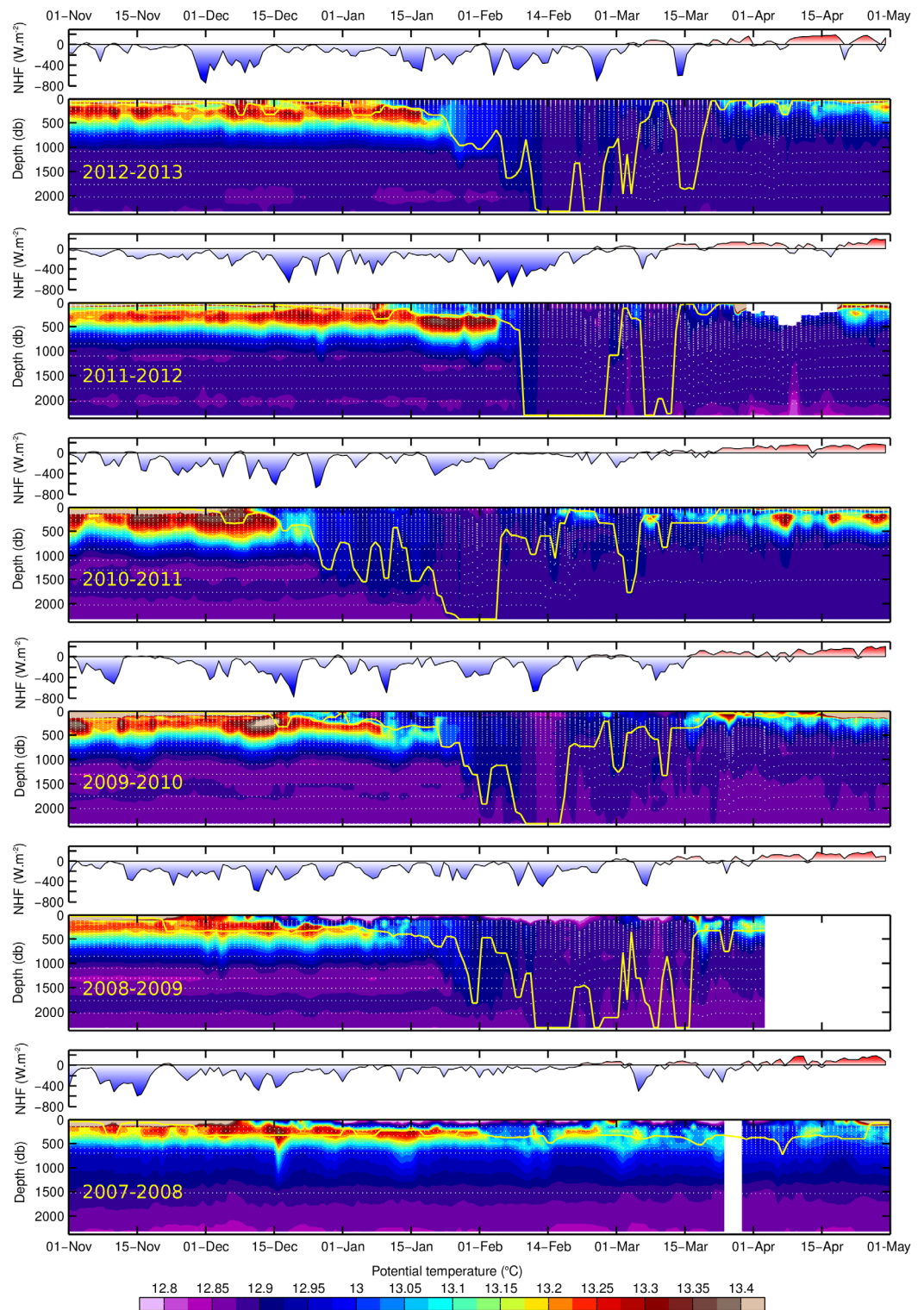


Figure 5. Mixed layer depth, potential temperature, and net atmospheric heat flux from ERA-Interim, from December to May for the 2007–2013 period. Horizontal gray-dotted lines show the depth of the mooring instruments. The yellow thick line indicates the mixed layer depth (see section 3.1 in the manuscript for a description of criterion chosen). Note the absence of temperature sensors between 2 and 150 m in 2007–2008 and 2008–2009, for these two periods only the SST sensor (1 m depth) was used, which might explain the “too cold” subsurface layer during winter when the sea surface experiences strong cooling.

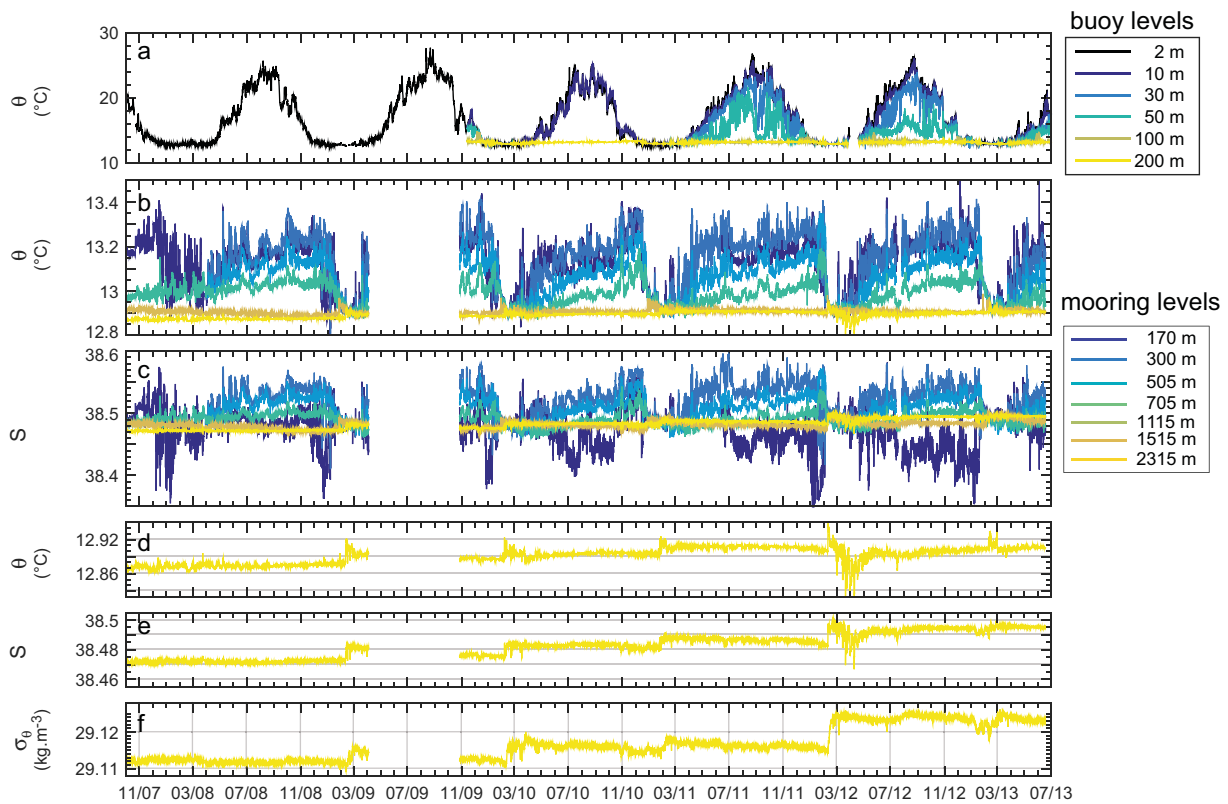


Figure 6. (a) Daily potential temperature from the sensors mounted below the surface buoy LION (from 2 to 200 m), (b) potential temperature, and (c) salinity recorded by Seabird Microcats from 170 to 2330 m between November–October 2007 and July 2013. (d) The near-bottom potential temperature, (e) salinity, and (f) potential density anomaly are also presented with a separate vertical scale.

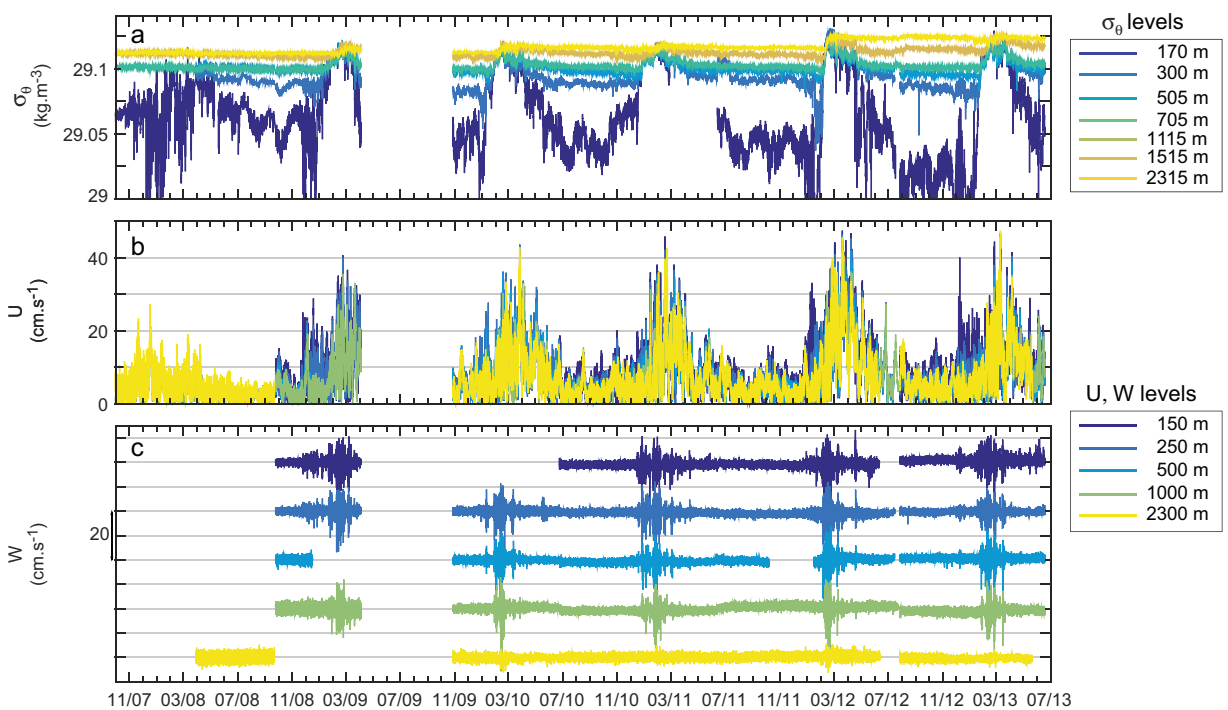


Figure 7. Daily potential density (a) recorded by Seabird Microcats from 170 to 2330 m between October 2007 and July 2013, with (b) horizontal and (c) vertical currents recorded at 250, 500, 1000, and 2330 m. Vertical currents are offset by $20 \text{ cm}\cdot\text{s}^{-1}$.

4.2.2. Winter Intermediate Water

Another interesting feature that emerges from the analysis of the multiyear time series is the presence of WIW advected at the mooring location before the deep mixing period in winters 2008, 2009, and 2010, and for the whole year in 2011, 2012, and 2013. This modal water mass can be detected thanks to its lower salinity (below 36.45, Figure 6c) and lower potential density (below 29.05 kg.m^{-3} , Figure 7a). Due to its lower density, the WIW increases the stratification in the deep convection area. Fresher WIW could definitely affect the depth of the deep convection, or even inhibit it. This modal water mass is generally formed around the deep convection area from the Balearic Sea to the Ligurian Sea [Millot, 1999]. Recently Juza *et al.* [2013] show that the continental shelf of the Gulf of Lions can be an important source of WIW. These results could change our vision of the links between the open ocean and the shelf, and particularly could highlight an important coupling of the two areas that has to be taken into consideration particularly by modelling simulations on deep convection and its interannual variability.

4.2.3. Horizontal Extent of the Deep Convection Area

Satellites can provide estimates of the sea surface chlorophyll-a (chl-a) based on ocean color images. These data provide essential information about the extension of the deep water formation zone. During winter-time, the Gulf of Lions is often characterized by low surface chl-a (Figure 8). This low chl-a patch indicates that the growth rate of the phytoplankton may be reduced in the euphotic layer, due to the active vertical mixing (Figure 7c), and/or that the phytoplankton is diluted in the whole mixed layer, that can reach 2300 m in February (Figure 5 and Table 4). No clear relationship exists between the low chl-a patch and the mixed layer depth. Here we propose to use glider data to determine surface chl-a thresholds delimiting the area of open-ocean deep convection in the Gulf of Lions.

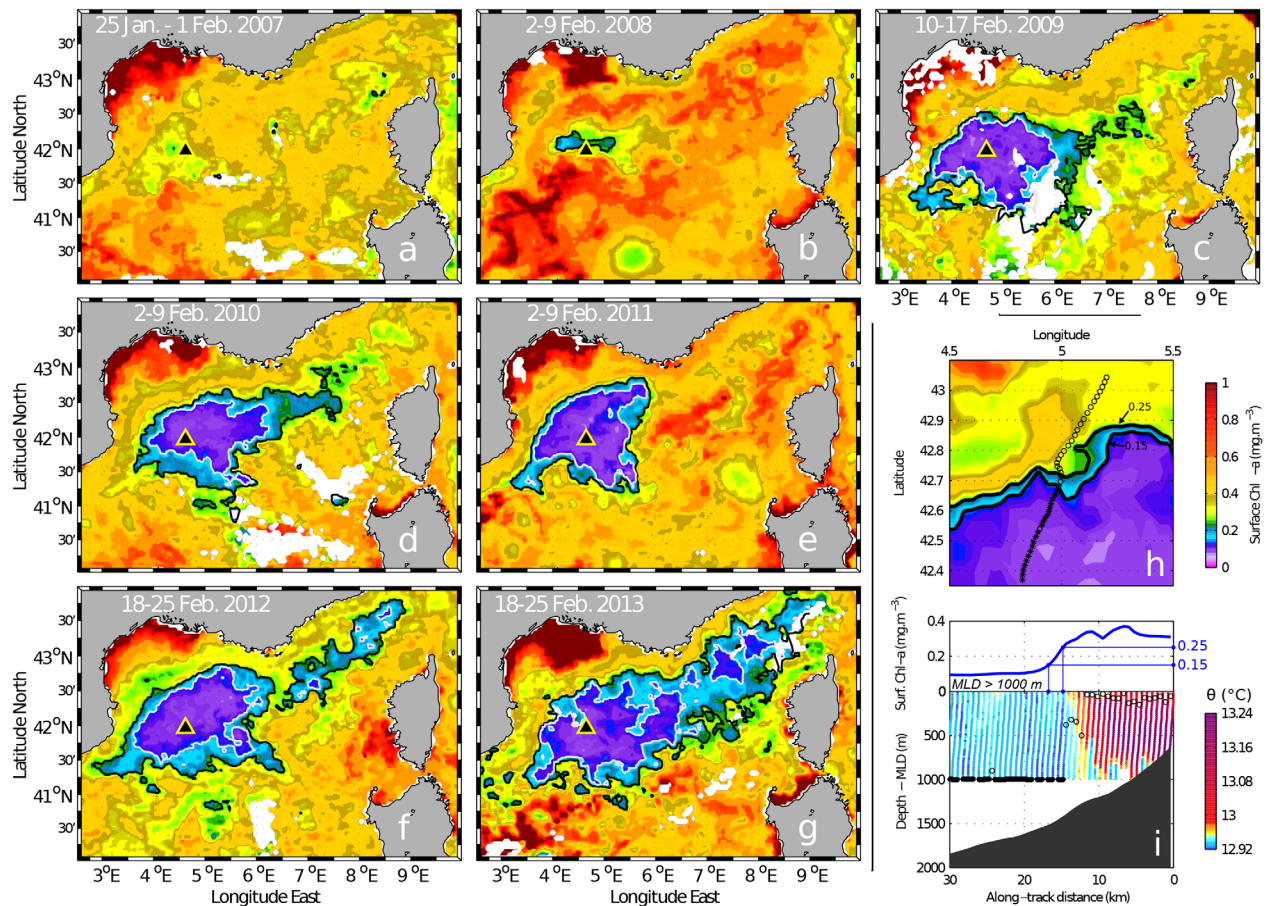


Figure 8. (a–g) Weekly surface chlorophyll images from MODIS for winter 2007 to 2013. (h) MODIS surface chlorophyll on 22 February 2012. The trajectory of a glider is shown for a 3 day interval centered on that date. Circles represent stratified profiles, whereas stars are for profiles having a MLD greater than 1000 m. (i) Surface Chlorophyll-a with the potential temperature profiles collected by the glider. The MLD from each glider profile (computed using a criterion at 0.02°C on the potential temperature and a reference at 10 m) is superimposed.

In February 2012, a glider crossed the chl-a front at the date of the satellite image shown in Figure 8f. The Figure 8h represents an enlargement of the satellite image and the glider trajectory within a 3 day interval centered on 22 February. The transition between the mixed conditions, characterized by low chl-a, and the stratified conditions occurs around the 1500 m isobath (Figure 8i). In this transition area, the chl-a estimated by the satellite ranges between ~ 0.15 and ~ 0.25 $\text{mg}\cdot\text{m}^{-3}$, and the MLD, estimated by the glider, reaches at least 1000 m. Furthermore, the potential temperature measured by the glider is close to the newly formed deep waters ($\sim 12.92^\circ\text{C}$). The glider cannot provide information below 1000 m, so we cannot detect the point where the MLD start reaching the seabed. However, the LION mooring was deployed for all these winters in the center of the deep convection, offering us a detailed timing of the evolution of the MLD.

The area of intense dilution (<0.15 $\text{mg}\cdot\text{m}^{-3}$) is not present in 2007 and 2008 (Figures 8a and 8b). The weakness of the deep convection is also confirmed by glider data. Indeed, five gliders deployed in the Gulf of Lions during the EGO2007 experiment from January 2007 to May 2007 recorded a maximal mixed layer of ~ 400 m depth [Testor *et al.*, 2007]. In winter 2008, another swarm experiment took place in the Gulf of Lions (EGO2008) with six gliders deployed in the Gulf of Lions from January to April. That year, a MLD of 1000 m depth was sporadically recorded mid-March by gliders ~ 50 km westward of the LION mooring location (near $42.1^\circ\text{N}/4.1^\circ\text{E}$), while the MLD was not deeper than 700 m depth at the LION mooring. These data seem in good agreement with the satellite image for the 8 day period going from the 2 to 9 February 2008 (Figure 8b), where the low chl-a patch defined by a criterion <0.25 $\text{mg}\cdot\text{m}^{-3}$ but >0.15 $\text{mg}\cdot\text{m}^{-3}$ extends westward of the mooring location. This might suggest that deep open-ocean convection is not homogeneous everywhere in the Gulf of Lions and could be triggered earlier, further west than the LION mooring, close to $42.1^\circ\text{N}/4.1^\circ\text{E}$.

Between winters 2009 and 2013, the area of intense dilution (<0.15 $\text{mg}\cdot\text{m}^{-3}$) varies between 13,000 km^2 in 2010 to a maximal value of 23,580 km^2 in 2013 (Figure 8 and Table 4). A criterion of surface chl-a <0.15 $\text{mg}\cdot\text{m}^{-3}$ seems to be more relevant to estimate the maximal horizontal extension of the deep convection area when cloud-free satellite images are available at the same period as the mooring records significant vertical mixing of the water column.

For winter 2009, 2010, and 2012, deep convection produces new WMDW significantly denser than the year before (Figure 6e). We estimate the formation rate of the new class of density for each of these three winters, by using a mean depth of the mixed patch of 2200 m and an area of intense dilution defined by the contour 0.15 $\text{mg}\cdot\text{m}^{-3}$ (delimiting the deep convection area). The results are summarized in Table 4 and range from: 1.14 Sv in 2009 (for the density class 29,114–29,116 $\text{kg}\cdot\text{m}^{-3}$), 0.91 Sv in 2010 (for the density class 29,116–29,119 $\text{kg}\cdot\text{m}^{-3}$) and 1.25 Sv in 2012 (for the density class 29,119–29,126 $\text{kg}\cdot\text{m}^{-3}$). The deep water formation rate in the northwestern Mediterranean Sea has the same order of magnitude as the other components of the circulation such as the volume transport associated with the Northern Current [Millot, 1999], and the inflow [Bryden *et al.*, 1994; Candela 2001], and outflow [Tsimplis and Bryden 2000; Candela 2001; Soto-Navarro *et al.* 2010] at the strait of Gibraltar. Our results agree well with other published estimates of the deep water formation rate in the northwestern Mediterranean Sea based on observations or models (0.3–2.4 Sv) [Tziperman and Speer 1994; Herrmann *et al.*, 2008; Schroeder *et al.*, 2008a; L'Hévéder *et al.*, 2013; Durrieu de Madron *et al.*, 2013; Somot *et al.*, 2016; Waldman *et al.*, 2016]. In this study, our estimates are likely to underestimate the formation rate of the new deep water due to different factors:

1. The upper limit for the chl-a criterion which is subjective and may vary from one year to another. Here we choose a minimal value of 0.15 $\text{mg}\cdot\text{m}^{-3}$, a larger value of 0.25 $\text{mg}\cdot\text{m}^{-3}$ would still be acceptable (compared to the MLD observed by glider) and would double our deep water formation area and dense water formation rate estimate;
2. They are only based on one instantaneous cloud-free image per year that could miss a part of the newly formed deep water already exported outside of the deep convection area.

4.2.4. Atmospheric Forcing and Water Column Stratification

The index of stratification IS(1000) from 2008 to 2013 is shown in Figure 9a (red line) with the error represented by the dotted purple lines. The higher the IS(1000) index value, the larger the integrated buoyancy losses must be to ensure convection down to 1000 m depth. Errors in our calculation of IS are nonnegligible for the first years (September 2007 to April 2009), with an order of 0.5 $\text{m}^2\cdot\text{s}^{-2}$. The stratification index IS(1000) varies between 0 $\text{m}^2\cdot\text{s}^{-2}$ in winter, when the water column is completely mixed, to 2 $\text{m}^2\cdot\text{s}^{-2}$ at the end of the summer, when the stratification of the water column is maximal. As the number of instruments on the mooring increase, errors on IS decrease (from 0.1 $\text{m}^2\cdot\text{s}^{-2}$ in 2010 to 0.02 $\text{m}^2\cdot\text{s}^{-2}$ or less in 2013).

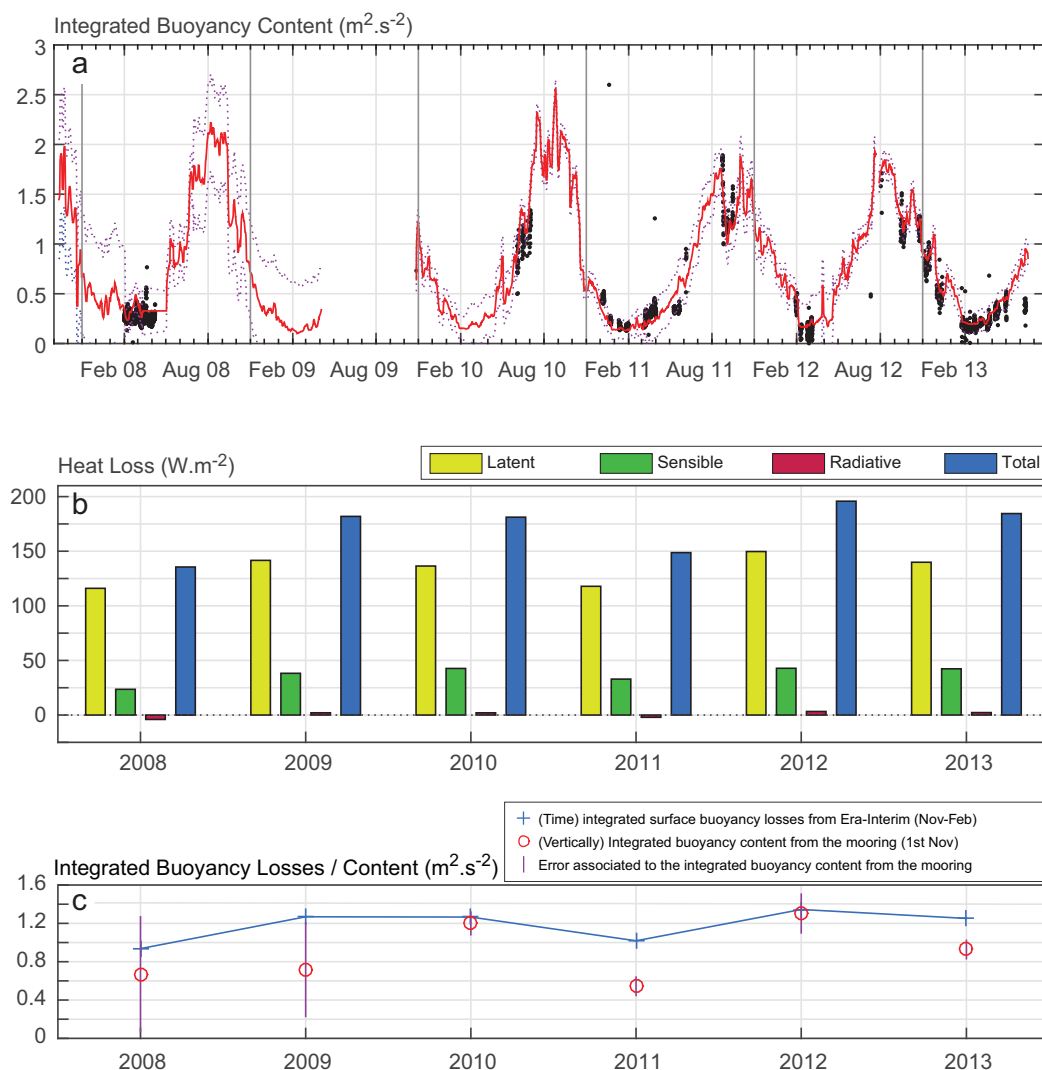


Figure 9. (a) Time series of the integrated buoyancy content of the first 1000 m IS(1000) in red, with the associated error (dotted purple line). The black dots correspond to IS(1000) calculated for vertical profiles carried out close to the mooring (<30km); (b) surface heat fluxes at the air-sea interface for the winter 2007–2008 to winter 2012–2013 from ERA-Interim (the integration period goes from 1 November to 1 March); (c) integrated surface buoyancy losses (blue) for the winter 2007–2008 to winter 2012–2013 from ERA-Interim (the integration period goes from 1 November to 1 March), with vertically integrated buoyancy content of the first 1000 m of the water column estimated on the 1 November of each year using the mooring (red circle). The purple vertical lines indicate the associated error (see section 3.3 for more details).

The different heat fluxes (latent, sensible, radiative) for winter 2008 to winter 2013 are presented together in Figure 9b. Mean heat fluxes are calculated from 1 November of the previous year to the end of February of the year under consideration. The strongest winter in terms of heat and integrated buoyancy losses is 2012 (196 W.m^{-2} , $1.35 \text{ m}^2\text{s}^{-2}$), while the weakest is 2008 (135 W.m^{-2} , $0.94 \text{ m}^2\text{s}^{-2}$). The net heat flux during wintertime is mainly dominated by the latent heat flux, between 75% (2010) and 86% (2008) of the total net heat flux, while the sensible heat flux represents only 17% (2008) to 24% (2010) of the total heat flux. The radiative heat flux is close to zero (between 1% and 3%).

IS(1000) is calculated for 1 November. As mentioned in the methods section, this index indicates how much the water column is stratified at the end of the preconditioning period, before the beginning of the deep vertical mixing phase. For all winters (2008–2013), we found that IS(1000) is inferior to the surface buoyancy losses integrated from 1 November to the end of February, indicating that atmospheric forcing is strong enough to explain that deep convection went down to 1000 m (Figure 9c). Another point is that 2011 appears to be the winter during which the water column is the least stratified at the beginning of November. This may

explain why deep convection occurs in 2011, while the mean winter heat losses are comparable to 2004, a year without any evidence of newly formed deep water on historical CTD profiles [Puig et al., 2013b].

As discussed in section 4.2.1, the heat losses in the beginning of February 2012 are very strong (Figure 5). The surface buoyancy losses integrated from 1 to 15 February are about $0.35 \text{ m}^2\text{s}^{-2}$, corresponding to a net heat flux of $-440 \text{ W}\cdot\text{m}^{-2}$. On 1 February, the stratification index $IS(1000)$ has a value of $0.45 \pm 0.10 \text{ m}^2\text{s}^{-2}$. By taking into account the $0.10 \text{ m}^2\text{s}^{-2}$ uncertainty on our calculation of $IS(1000)$, we see that the surface buoyancy losses integrated from 1 to 15 February can explain by themselves why the MLD deepened by 2000 m at the beginning of February 2012. For the other winters, the mixed layer went from the LIW layer to the bottom in a period ranging between 2.5 weeks and 1 month, while in 2012 it took only 5 days.

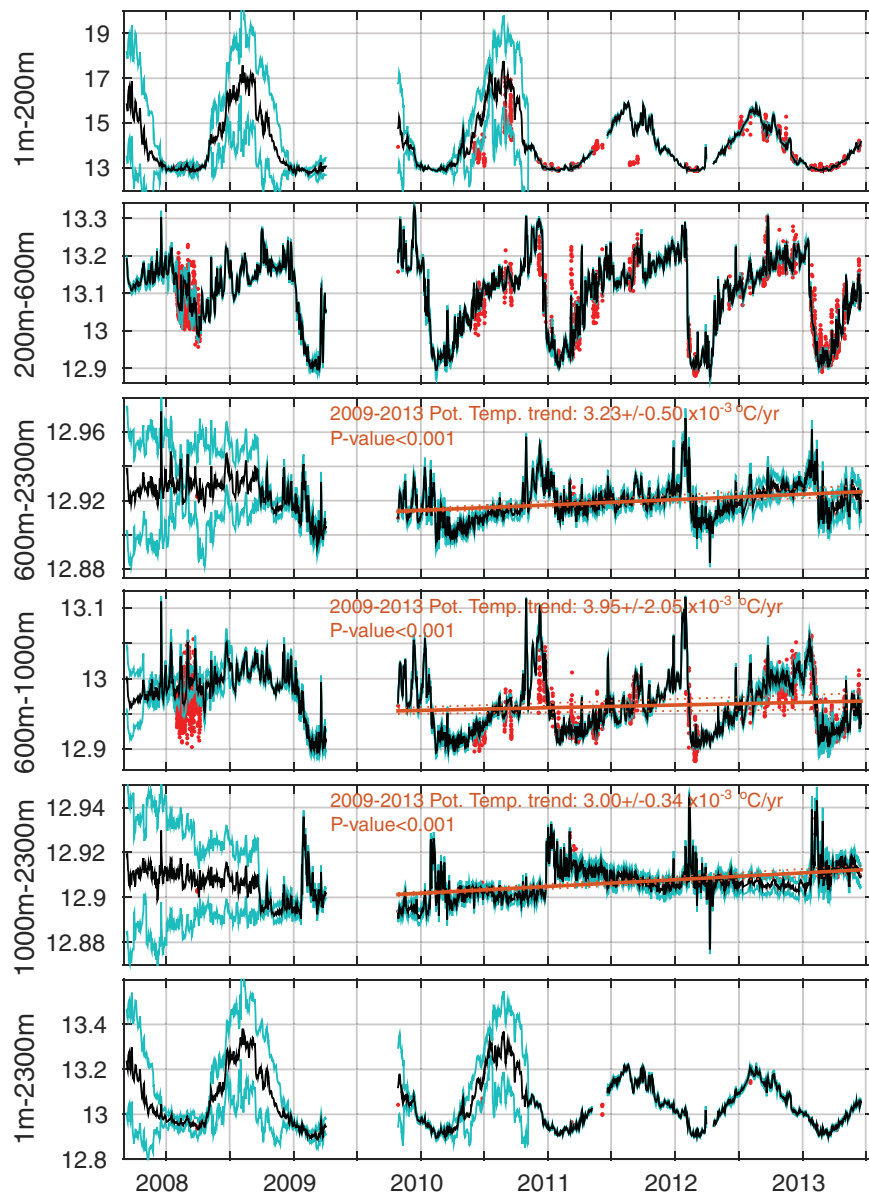


Figure 10. Temporal evolution of the mean potential temperature ($^{\circ}\text{C}$) of the water column and specific layers at the LION mooring. The error due to the vertical integration is represented by the blue line. The red dots correspond to the mean potential temperature calculated with vertical profiles close to the mooring ($<30 \text{ km}$). From October 2009 to July 2013, linear trends are estimated fitting a straight orange line by means of least squares. The slope of the fit represents the observed trend. 95% confidence intervals for the trends are calculated considering a student's t test.

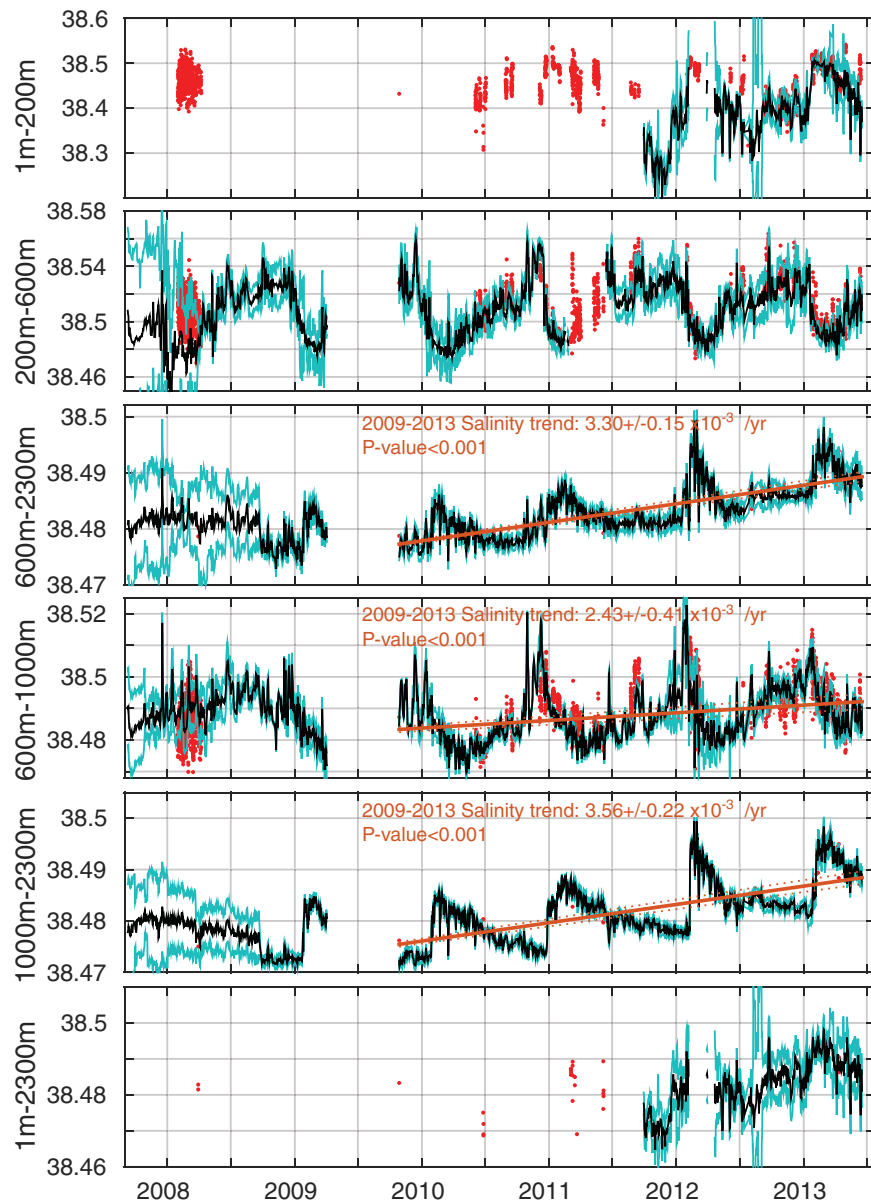


Figure 11. Equivalent to Figure 10 but for the mean salinity.

4.3. Modification of Water Masses Characteristics

We analyze in this section the evolution of the heat and salt content of the water column and the thermohaline characteristics of the deep water masses from 2007 to 2013.

4.3.1. Evolution of the Heat and Salt Content of the Water Column

Figures 10–12 show the mean potential temperature, salinity, and potential density for the main water masses of the WMED: the Atlantic Water (AW, 0–200 m), the Levantine Intermediate Water (LIW, 200–600 m), and the deep waters (WMDW, 600–2300 m). A distinction is made for the deep waters between 600 and 1000 m (oWMDW) and between 1000 and 2300 m (nWMDW), as θ - S diagrams show since 2005 the appearance of newly formed deep water masses below 1000m [López-Jurado et al., 2005; Salat et al., 2006; Schroeder et al., 2006; Puig et al., 2013b] (Figure 13).

4.3.1.1. The Surface Layer 0–200 m

The daily averaged data at the mooring (dark line) are represented together with data from CTD casts from research vessels, gliders, and profiling floats (red dots). Errors due to the limited number of vertical levels for the mooring are also indicated as cyan lines. We can clearly see a seasonal cycle in the mean potential

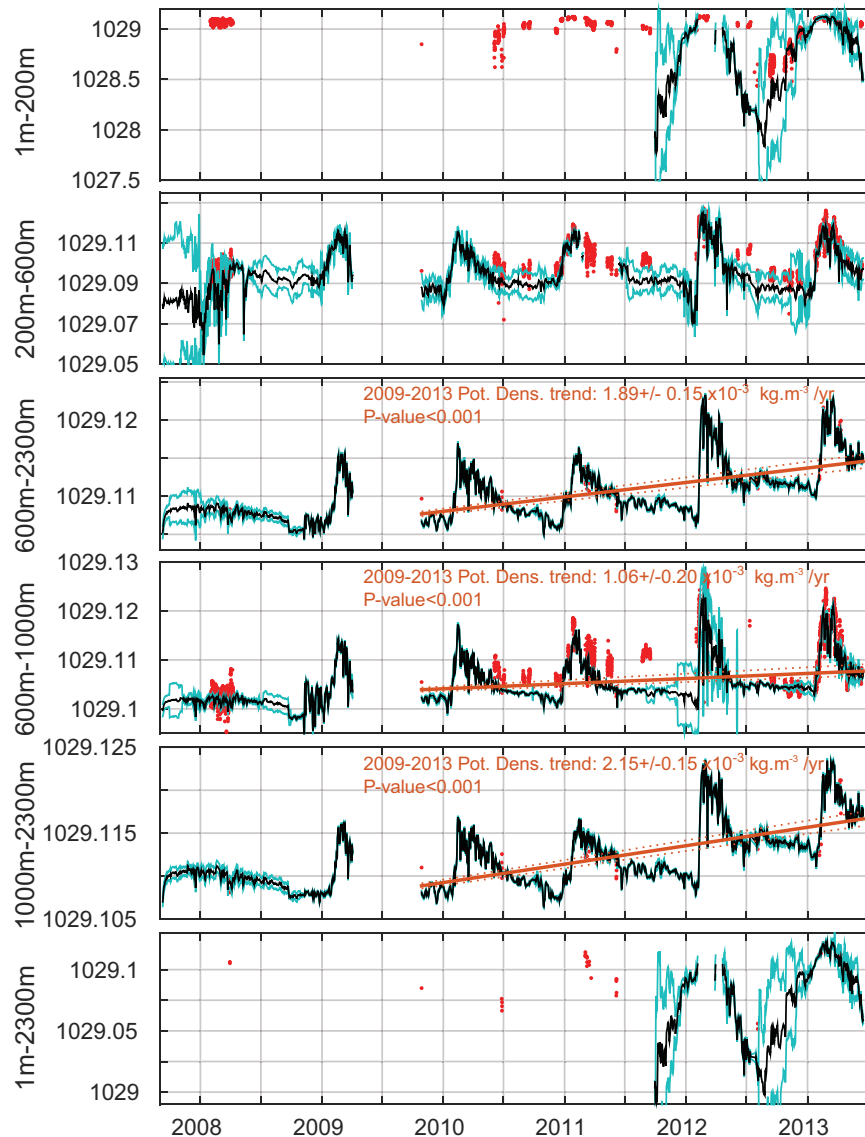


Figure 12. Equivalent to Figure 10 but for the mean potential density ($\text{kg}\cdot\text{m}^{-3}$).

temperature of the surface layer (1–200 m) varying from $13.0 \pm 0.2^\circ\text{C}$ in winter to $17 \pm 2^\circ\text{C}$ in summer. The higher error during summertime (Figure 10) is mainly due to the low number of instruments in this layer, the strong surface gradient in potential temperature associated with the summer thermocline is not captured correctly. In winter, the surface layer is homogeneous in potential temperature and thus the errors are negligible. After the addition of temperature sensors under the LION buoy in November 2010 (Table 2), the errors, associated with the vertical interpolation of the potential temperature records, become negligible in both winter and summer. Since a conductivity sensor has been installed on the LION surface buoy only from September 2011, mean salinity and density are not available for the layer 1–200 m or 1–2300 m for the 2007–2011 period. The decrease in the error on the mean salinity and potential density seen in 2011 and 2012 is due to the winter mixing, which homogenize the upper ocean.

4.3.1.2. The Intermediate Layer (200–600 m)

The heat and salt content variability of the intermediate layer (200–600 m) at the LION mooring site is mainly driven by the deep convection events with a $\sim 0.3^\circ\text{C}$ decrease in potential temperature (Figure 10) and ~ 0.05 decrease in salinity (Figure 11) in winter, when the deep convection reaches the seabed. The small number of conductivity sensors (see Table 2) explains why before April 2008, the error on the mean salinity is larger than the error on the mean potential temperature.

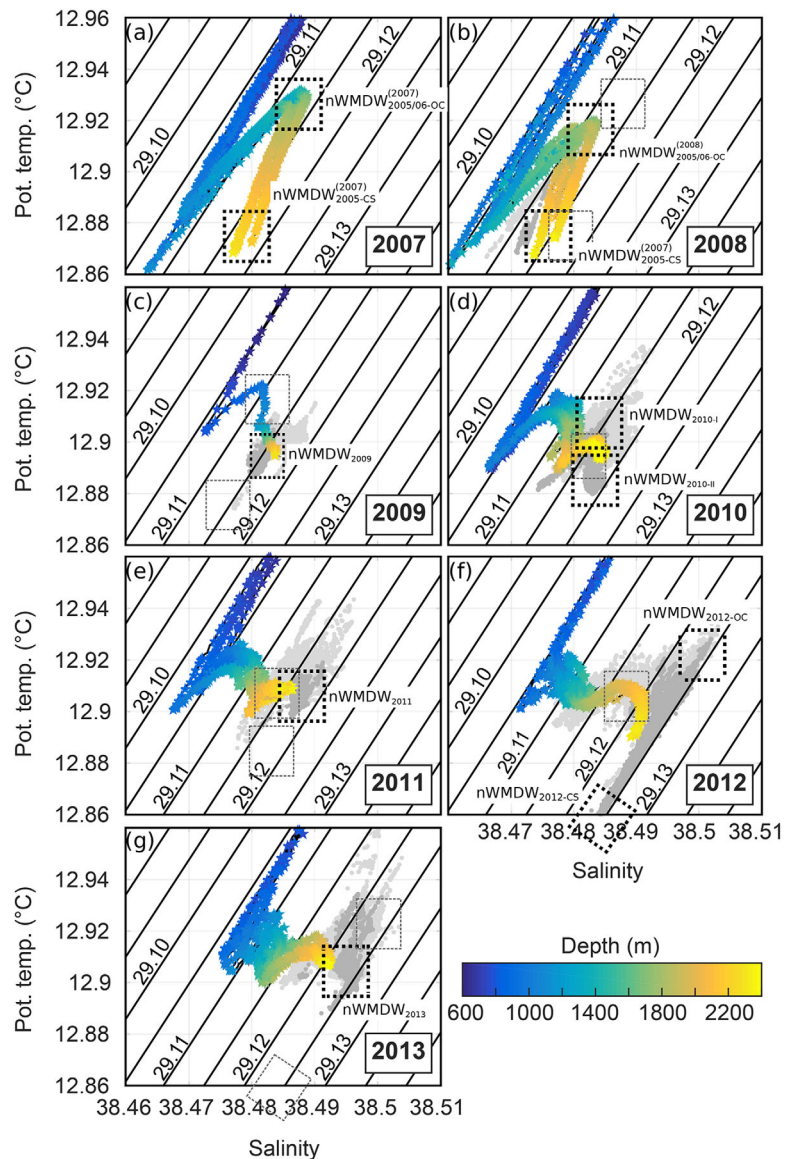


Figure 13. θ - S diagrams of WMDW from CTD stations highlighting the interannual variability of the deep stratification and θ - S characteristics of the WMDWs from 2007 to 2013 in the deep convection area, with the formation of new WMDW in 2009, 2010, 2011, 2012, and 2013. The new WMDWs are labeled (see section 4.3.3 for explanation) and their wintertime θ - S characteristics, observed by the mooring, are indicated by a black-dashed box. For visual reference, each year the θ - S characteristics of the WMDW of the previous winter are shown as a light gray box. The dark gray (resp. light gray) dots show the θ - S properties recorded by the 2300 m (resp. 1500 m) Microcat at the end of the vertical mixing phase. The differences in θ , S , and σ_θ between the CTD stations carried out in summer (in color) and the wintertime observations (in February) from the mooring instruments (light and dark gray dots), illustrate the effects of the isopycnal mixing on the WMDW θ - S characteristics. The isopycnal mixing of the WMDW is associated with the spreading of the newly formed deep water and the restratification of older WMDW surrounding the deep convection zone. The colorbar shows the pressure on the different CTD stations carried out close (<30km) to the LION mooring: (a) DOCONUG2007; (b) DOCONUG2008; (c) 42N5E in 2009; (d) MOOSE_GE_2010; (e) MOOSE_GE_2011; (f) MOOSE_GE_2012; and (g) MOOSE_GE_2013.

No clear trend of warming of the 200–600 m layer appears for the 2007–2013 period. After the intense vertical mixing period of the deep convection reaches the bottom, the restratification of the 200–600 m layer to its preconvection potential density level (29.09 kg.m^{-3}) takes between 5 and 6 months (Figure 12).

4.3.1.3. The Deep Layer (600–2300 m)

The spreading of the newly formed deep waters can be seen in the 1000–2300 m layer, in Figure 12. At the end of the intense vertical mixing period, the potential density reaches a local maximum. Once the intense atmospheric forcing has stopped, the potential density at the mooring location begins to decrease, indicating the spreading of the newly formed deep waters and their mixing with the older deep waters found in

the surrounding area. It takes between ~ 4 months (in 2012) and ~ 6 months (in 2010) for the deep layers to dissipate 50% of their potential density increase due to bottom-reaching convection. The absence of deep convection in 2007 and 2008 explain why the important seasonal variability of the mean potential density of the 1000–2300 m layer, $O(0.01 \text{ kg}\cdot\text{m}^{-3})$, is seen only since 2009. This seasonal variability in the mean potential density of the deep layer is due to new deep (i.e., dense) water formation, the spreading of this new deep water and the restratification of older deep water.

The warming and salting of the deep layers (600–2300 m) cannot be clearly seen for the 2007–2008 period due to a too large error on the heat and salt content. However, in September 2008, the addition of instruments on the line considerably reduces the error on the estimation of the heat and salt content of the deep layers (Figures 10 and 11). The formation of warmer and saltier deep waters after each deep convection event can be seen as an injection of heat and salt in the deep ocean. From October 2009 (after the 6 month observational gap) to July 2013, linear trends are estimated fitting a straight line by means of least squares, for the potential temperature, salinity, and potential density of the deep water. The slope of the fit represents a trend or a mean annual change. The 95% confidence intervals for the trends are calculated using a student's t test. All the trends in this study are significant (slope different from 0) as their p values are lower than 0.001.

Between October 2009 and July 2013, the linear trends, calculated with a 95% confidence interval, in the deep layer corresponding to the nWMDW (1000–2300 m are: $3.0 \pm 0.3 \times 10^{-3} \text{ }^\circ\text{C}/\text{yr}$ for the potential temperature (Figure 10), $3.6 \pm 0.2 \times 10^{-3}/\text{yr}$ for the salinity (Figure 11) and $2.2 \pm 0.2 \times 10^{-4} \text{ kg}\cdot\text{m}^{-3}/\text{yr}$ for the potential density (Figure 12). The increase in heat (salt) for the 600–2300 m layer is about $3.2 \pm 0.5 \times 10^{-3} \text{ }^\circ\text{C}/\text{yr}$ (resp. $3.3 \pm 0.2 \times 10^{-3}/\text{yr}$). Vargas-Yanez *et al.*, found trends of $1.2 \pm 1.0 \times 10^{-3}/\text{yr}$ for the salinity and $0.28 \pm 0.23 \text{ W}\cdot\text{m}^{-2}$ for the heat content, corresponding to a trend in potential temperature of $1.1 \pm 0.9 \times 10^{-3} \text{ }^\circ\text{C}/\text{yr}$ (using a mean potential density of $1029 \text{ kg}\cdot\text{m}^{-3}$, a mean potential temperature of 12.8°C , and a mean salinity of 38.4).

We found a warming and salting rate for the 2009–2013 period three times higher than the one previously established by Vargas-Yanez *et al.* [2010b] in the Gulf of Lions for the 1952–1995 period. A first explanation for these different trends lies in the different periods and the different methods used: Vargas-Yanez used a 43 year reconstructed time series from CTD casts, while in this study we used a 4 year time series from mooring data. Observations of deep convection were sparse before the 2000 s, therefore we cannot be sure that five consecutive years of deep convection, such as the one presented in this work, did not happen in the past.

Every deep convection event induces an injection of heat and salt in the deep layer due to the vertical mixing of the LIW with the fresher and colder deep water. Different factors can explain the formation of warmer and saltier deep water compared to the 43 year period studied by Vargas-Yanez, such as changes in the stratification of the surface and intermediate layers. For the same atmospheric forcing, a less stratified AW/LIW layer would allow the vertical mixing to reach the bottom more quickly, and the continuous buoyancy losses would continue decreasing the temperature of the whole water column, leading to colder deep water. The reasons for these changes in the AW/LIW stratification are still not clearly understood. The changes in the θ - S characteristics of the AW and LIW can be due to increasing temperature and salinity in the inflowing AW at Gibraltar Strait [Millot, 2007], changes in large-scale atmospheric patterns [Josey *et al.*, 2011], and an accumulation of heat and salt in the intermediate layer due to the absence of deep convection during the 1990s [Herrmann *et al.*, 2010] and the propagation of the EMT to Western Mediterranean Sea [Schroeder *et al.*, 2010].

4.3.2. Variability and Transients in the Bottom Layer

4.3.2.1. Stepwise Increases and Long-Term θ - S Evolution of the nWMDW

The stepwise increase in bottom waters characteristics can be noticed for five consecutive years (2009–2013) as positive jumps in θ and S (Figures 6d and 6e, Table 4), resulting from deep convection events that reach the bottom in February. The formation of these warmer and saltier deep waters can be seen as an injection of heat and salt in the deep ocean, leading to the observed trends (detailed in the previous subsection) in the potential temperature, salinity, and potential density of the deep water.

If the long-term increase in salinity and potential density of the deep layers seems to be strongly related to the recurrent formation of salty deep waters, the warming trend of the nWMDW can be reduced by very strong events of deep convection when the mixed layer depth reaches the bottom and the strong

buoyancy loss continues to decrease the potential temperature of the mixed layer and therefore of the newly formed deep water by $O(0.01)$ degree. During this period of intense vertical mixing (9–12 days, Table 4), the salinity remains relatively constant, but the potential temperature of the bottom waters undergoes a significant decrease (Figures 6d and 6e) ranging from 0.012°C in winter 2011 to 0.032°C in winter 2012 (Table 4). This potential temperature decrease induces an increase in the potential density of the newly formed deep waters between $0.003\text{ kg}\cdot\text{m}^{-3}$ in winter 2011 to $0.009\text{ kg}\cdot\text{m}^{-3}$ in winter 2012 (Figure 6f).

Another deep mooring part of the HydroChange program monitors the evolution of the deep waters in the Gulf of Lions since autumn 2006 (located at $45^{\circ}\text{N}/5^{\circ}\text{E}$, at 2400 m depth, about 30 km.s east of the LION mooring location). From data collected at this mooring, *Schroeder et al.* [2013] also noticed the abrupt positive jumps in θ and S occurring in February 2009, 2010, and 2011, and the subsequent decrease in potential temperature. The two previous winters (2007 and 2008) show rather stable near-bottom θ and S at $12,869 \pm 0.005^{\circ}\text{C}$ and $38,479 \pm 0.002$. We interpret this decrease in potential temperature of the mixed layer, already seen by *Schroeder et al.* [2013], as the effect of intense net heat losses after that the MLD has reached the seabed. The absence of an increase in the salinity of the bottom waters at the same time can be explained by the dominance of the heat fluxes on the wintertime buoyancy fluxes [*Grignon et al.*, 2010]. As already discussed in section 4.1, the salinity of the newly formed deep waters is mostly set by the salt content of the water column before convection, while its potential temperature results from a combination of the initial heat content of the water column and of the surface heat fluxes.

4.3.2.2. θ - S Inhomogeneity of the New WMDW Formed by Deep Convection

On 25 March 2010, the potential temperature of the bottom waters undergoes a sharp decrease ($\approx 0.02^{\circ}\text{C}$, Figure 2d), resulting in an increase in the potential density ($0.002\text{ kg}\cdot\text{m}^{-3}$, Figure 2f). At that moment, the water column is already stratified and the atmospheric forcing only cannot explain this potential temperature change (Figure 3d). Then the potential temperature progressively increases until reaching an equilibrium state in August 2010 (Figure 2d). No similar signal is recorded by the conductivity sensors. The high salinity values of the deep waters measured after February 2010 have never been recorded since the first deployment of the mooring in November 2007 (Figure 6e). This secondary newly formed deep water mass is characterized by a colder potential temperature, a similar salinity, and a higher potential density. This new WMDW, observed from 25 March 2010, is therefore distinct from the main one observed between 18 February and 25 March 2010 (Figures 2d and 2e). The linear decrease in potential density between April and August 2010 observed on the near bottom Microcat (Figure 2e) is associated with a period of intense horizontal currents (Figure 3b). This is certainly the indication of the mixing between these two different newly formed deep waters, as the salinity remains almost constant from April to August.

This colder newly formed deep water is detected one month after the last vertical velocities are recorded at 1000 m depth on 18 February (Figure 3c). As both new water masses have the same salinity (set by the salt content of the water column before convection, as described in section 4.1), this new water mass should have been formed within the deep convection zone. The only differences between the two new water masses are their temperature, indicating that the two formation sites could have experienced slightly different atmospheric conditions and/or the preconvection water column could have different θ - S characteristics. *Lacombe et al.*, [1985] already suggested heterogeneity inside the mixed patch with different water-mass formed in different parts of the cyclonic gyre.

Considering similar buoyancy fluxes acting in two locations characterized by different stratifications, the deepening of the mixed layer will be faster where the stratification is lower. Such local modification of the stratification could be induced by the presence of (sub) mesoscale eddies that help the mixed layer deepening [*Lherminier et al.*, 1999; *Legg and McWilliams*, 2001; *Bosse et al.*, 2015]. Furthermore, a shallower bottom depth could allow the MLD to reach the seabed earlier. In this case, the entire homogeneous water column could be exposed to severe heat losses for a longer period of time. This would finally lead to a stronger potential temperature decrease and to the formation of colder and denser deep waters.

4.3.2.3. WMDW Formed by Dense Shelf Water Cascading

Another remarkable signal can be noticed between March 2012 and May 2012. It is characterized by a sharp decrease of the bottom potential temperature and salinity and high-frequency fluctuations in potential temperature and salinity (Figures 6d and 6e). This high-frequency variability is not seen in the potential density time series (Figure 6f), and indicates two distinct water masses characterized by different potential temperature and salinity (discussed more in details in the next section, 4.3.3). The origin of the bottom waters

characterized by a lower potential temperature and salinity has been identified as the result of dense shelf water cascading [Durrieu de Madron *et al.*, 2013]. The peculiar atmospheric conditions of winter 2012 indeed triggered a massive formation of dense waters over the continental shelf that overflowed the shelf edge and cascaded down to the bottom of the Gulf of Lions basin.

4.3.3. Evolution of the Western Mediterranean Deep Water(s)

Although the open-ocean deep convection is the main mechanism for the renewal of the WMDW, dense shelf water cascading can have an influence on WMDW, as it was first suggested by Bethoux *et al.* [2002], and sketched in Figure 1 of Puig *et al.* [2013a]. Puig *et al.* [2013b] highlight the persistence in the deep waters since winter 2005 of a θ - S anomaly related to dense shelf water cascading. The coexistence of deep waters formed by deep convection and by dense shelf water cascading can be clearly seen on a θ - S diagram with a V-shape linking the denser deep waters formed by cascading and the deep waters formed by open-ocean convection. Several authors reported this shift in deep waters characteristics since 2005 [López-Jurado *et al.*, 2005; Canals *et al.*, 2006; Schroeder *et al.*, 2006, 2008b; Smith *et al.*, 2008; CIESM, 2009].

In 2007, CTD stations made in the Gulf of Lions clearly show three different deep water masses (Figure 13a) and an inverse V-shape structure below the Levantine Intermediate Waters (>600 m). One can clearly see the stacking of three different water masses (indicated by a θ - S extremum) with the “old” WMDW (oWMDW, between 800 and 1400 m), the “new” WMDW formed by deep convection in winters 2004/2005 and 2005/2006 (nWMDW_{2005/06-OC}⁽²⁰⁰⁷⁾, between 1400 and 1900 m) and the “new” WMDW formed in winter 2004/2005 by dense shelf water cascading (nWMDW_{2005-CS}⁽²⁰⁰⁷⁾, between 2000 m and the bottom). We use superscript in order to define the year when the deep waters are observed. Thermohaline characteristics of the deep waters change from year to year due the permanent turbulent mixing, which tends to homogenize the deep layers and progressively fade the signal of the different deep water masses. For example, in 2005 the θ - S characteristics of the bottom waters (nWMDW_{2005-CS}) recorded in the Gulf of Lions by Schroeder *et al.* [2006] were close to $\theta = 12.76^\circ\text{C}$ and $S = 38.46$, while 2 years later the observed θ - S characteristics of this water mass are less pronounced ($\theta = 12.87^\circ\text{C}$ and $S = 38.48$). The year to year evolution of a specific deep water mass can be tracked on θ - S diagrams in particular during years without wintertime deep convection events.

In 2008 (Figure 13b), CTD casts reveal the fading of the deep waters signal, especially for the deep water mass found between 1400 and 1900m. The potential temperature of the nWMDW_{2005/06-OC}⁽²⁰⁰⁸⁾ decreases by 0.02°C in 1 year, while the salinity decreases about several thousandths (same order of magnitude as our confidence in the calibration of the CTD).

In July 2009, the deep waters are homogenized with a less pronounced V-shape structure. This year a new thermohaline anomaly appears on the θ - S diagram. On the last 300 m of the water column, a warmer water mass can be seen (Figure 13c). As presented in section 4.2, 2009 is a year of bottom-reaching deep convection (Figure 5) characterized by an increase in the potential temperature and the salinity of the bottom waters after the deep convection event (Figures 6d and 6e). The range of near-bottom salinity and potential temperature recorded at 2300 m depth just at the end of the vertical mixing is shown by the dark gray dots in Figure 13c. These potential temperature and salinity correspond to the characteristics of the newly formed deep water of 2009 (nWMDW₂₀₀₉) at the time of its formation, while CTD casts from July reveal less marked bottom water characteristics, a consequence of their mixing with “older” deep waters.

The detection of newly-formed deep water on a θ - S diagram is relatively straightforward in the months following the deep convection period (appearance of a new extremum in the θ - S diagram). But identification of the older “vintage” of deep water masses is more difficult on CTD profiles carried out in summer when the deep water masses have started to mix with each other. However, a local maximum in potential temperature between 1000 and 1400 m depth can be noticed in the θ - S diagram in 2009 (Figure 13c), suggesting the presence of a water mass with θ - S characteristics close to nWMDW_{2005/06-OC}⁽²⁰⁰⁸⁾.

In June 2010, CTD casts still show the inverse V-shape structure between 800 and 1800 m, but a second thermohaline structure appears below 1800 m, also under the shape of an inverse V. One can relate this second V-shape with the particular characteristics of the newly formed deep waters of 2010. As discussed in the previous section (4.3.2), two different deep water masses nWMDW_{2010-I} and nWMDW_{2010-II} could have been formed in winter 2010 (indicated by the two dark rectangles in Figure 13d). These two water masses can be seen on the temporal evolution of the bottom potential temperature in March 2010 (Figure 2d). The

similar salinity and the different potential temperature explain why during the summer cruise a second inverse V-shape structure can be seen at the end of θ -S diagram tail. A possible explanation for the decrease of the vertical gradient of θ in the bottom layer in June compared to March can be found in the (isopycnal) mixing that constantly tends to homogenize the deep waters, during that time the horizontal currents are particularly important (Figure 7b).

In winter 2011, deep convection reaches the seabed (Figures 5 and 7c). Warmer and saltier deep waters are produced (Figure 13e). This new bottom water mass (nWMDW₂₀₁₁) is also observed on CTD casts performed in June 2011.

The first winter of concomitant open-ocean deep convection and dense shelf water cascading since 2006 is observed in winter 2012 [Durrieu de Madron *et al.*, 2013], In addition to the mooring data, where a significant drop of potential temperature and salinity can be noticed in April 2012, the presence of the dense waters of shelf origin can clearly be seen on CTD casts performed in July 2012 (Figure 13f). A new inverse V-shape structure appeared in the θ -S diagram below 1600 m, similar to the deep stratification after winter 2005. This thermohaline anomaly extends over more than 600 m on CTD casts made close to the mooring location. The shape of the anomaly can be related to the new deep waters formed in winter 2012 by open-ocean deep convection (nWMDW_{2012-OC}) and by cascading from the shelf (nWMDW_{2012-CS}) as indicated by the gray dots in Figure 13f. Extrema in θ and S associated with the dense shelf waters are, respectively, $\theta = 12.80^\circ\text{C}$ and $S = 38,479$.

In winter 2013, no deep water formed by dense shelf water cascading is detected. After the deep convection event of February 2013, there is no sudden freshening of the bottom layer (Figure 6), as in March–April 2012. Winter 2013 is a winter of deep convection with a mixed layer reaching the seabed (Figure 5) but the newly formed deep water nWMDW₂₀₁₃ cannot be distinguished from the nWMDW₂₀₁₂ by using only θ -S diagrams of the 2013 summer CTD (Figure 13g). The changes in potential density and in salinity of the bottom layer, after 2013 deep convection event, are the smallest since the first recording of deep convection in 2009 (Figure 6e and Table 4). For winter 2013, the salinity of the bottom water increases by 0.004, and the potential density by $0.003 \text{ kg}\cdot\text{m}^{-3}$. As for all the previous years, the deep layer is not uniform. A “smooth” inverse V-shapes can be seen below 1600 m indicating that the nWMDW formed in 2012 still influence the deep stratification in the Gulf of Lions.

5. Conclusions

For the first time, an observing system monitored continuously the deep convection phenomena providing invaluable hydrological observations of 6 years of open-ocean deep convection (October 2007 to July 2013) from surface moored buoy MF-LION and deep mooring LION located in the center of the open-ocean dense water formation zone of the Northwestern Mediterranean Sea. The first winter in 2008 is characterized by deep convection reaching ~ 1000 m depth, and the next five winters (from 2009 to 2013) are characterized by deep convection reaching the seabed, found at a depth of 2300 m. Using glider, moored, and satellite observations, we propose to estimate the maximal extent of the area of deep convection in the Gulf of Lions. We delimit the deep convection area by a surface chlorophyll criterion of $0.15 \text{ mg}\cdot\text{m}^{-3}$, ranging from about $13,000 \text{ km}^2$ in winter 2010 to $24,000 \text{ km}^2$ in winter 2013. Assuming a mean depth of 2200 m, we use these surfaces to estimate a formation rate of the new denser class of deep water that appear in 2009, 2010, and 2012. This formation rate, associated with the higher density class observed in winter, range between 0.9 Sv in 2010 and 1.25 Sv in 2012.

The LION mooring is a unique observing platform to study the temporal evolution of the mixed layer in an area where the MLD can reach the seabed, found at a depth of 2300 m. A secondary vertical mixing period generally occurs in March after the end of the main event of deep ocean convection. This short mixing phase (2–4 days) happens right after the onset of the restratification. The water column is weakly stratified at that time and can be easily destabilized. A period between 3 and 6 days of buoyancy losses, due to intense and frequent wind bursts (Mistral/Tramontane), can lead to a fast deepening of the mixed layer (> 1500 m). The long restratification and spreading times, which can be observed after each winter of deep convection, suggest that the restratification/spreading phase is still active at the beginning of the next deep convection event. The overlapping of the three phases of the deep convection process suggests a “memory effect” of the water column. Further studies need to be conducted to investigate the role of

(sub-)mesoscale eddies for the restratification of the area, the spreading of the newly formed deep waters, and also for the preconditioning of the area.

Observations from the LION mooring confirm that the salinity of the newly formed deep waters is essentially controlled by the salinity content of the mixed layer, as already suggested by *Grignon et al.* [2010]. However, the potential temperature of the newly formed deep water is driven by the heat content of the mixed layer and by the surface buoyancy loss during the deep vertical mixing. Once the mixed layer reaches the seabed, the strong surface buoyancy losses act to decrease the potential temperature of the mixed layer, and therefore of the newly formed deep water by $O(0.01)$ degree.

These sudden inputs of salt and heat in the deep water, after each event of deep convection, are responsible for the salting and heating of the deep water. For the period 2009–2013, the mean annual change in salinity is $3.3 \pm 0.2 \times 10^{-3}/\text{yr}$ for the 600–2300 m layer, while the trend in potential temperature is $3.2 \pm 0.5 \times 10^{-3}/\text{yr}$ for the 600–2300 m layer. These trends indicate warming and salting of the deep layer (600–2300 m) for the 2009–2013 period three times higher than the one previously established by *Vargas-Yanez et al.* [2010b] in the Gulf of Lions for the 1952–1995 period, which could be due to recent changes in the stratification of the surface and intermediate layers. These observations suggest an important role of recurrent events of deep convection in accelerating the warming and salting of the Western Mediterranean Deep Water.

Newly formed deep waters have been detected after every winter of deep convection from 2009 to 2013. In winter 2010, we observed for the first time two distinct new deep water formed by deep convection during the same winter. They present a different potential temperature but a similar salinity, suggesting that both might have been formed within the cyclonic gyre but in different locations. In 2012, two new deep waters have also been detected at the mooring location. One was identified as a result of open-ocean deep convection, while the other is the result of dense shelf water cascading that occurred in winter 2012 [*Durrieu de Madron et al.*, 2013].

Although the persistence of the different deep waters in the WMED could be partly studied with the large number of observations collected during the last decade, the LION mooring offers new insights into deep waters dynamics, a major element of the thermohaline circulation of the Mediterranean Sea. The 7 year of θ - S diagrams clearly shows the successive appearance of new deep water masses after each deep waters formation event reached the seabed. However, after each winter of deep convection, the newly formed deep waters spread into the whole basin and progressively mix with the former deep waters. This explains the “attenuated” characteristics of the deep waters recorded during the summertime CTD-surveys, compared to winter extrema recorded at the LION mooring. Several water masses composing the WMDW in the western Mediterranean have been found to persist for several years since 2005 and might be related to a mixing in the deepest layers less intense than previously thought, or to an increasing volume of newly formed deep waters during the last years.

Appendix A: The LION Mooring Line: Instruments and Calibration

RBR sensors TR-1050/1 and TR-1060 (temperature recorders manufactured by RBR (<https://rbr-global.com/>)) were used between 150 and 700 m depth until June 2011, and were replaced afterward by SeaBird Temperature Logger SBE56. SeaBird Microcat SBE37 (conductivity-temperature-pressure recorders) were located all along the line between 150 m depth and 2300m. Nortek Aquadopp were deployed since LION3 (September 2008) at five levels measuring horizontal and vertical currents, while there were only two Aanderaa RCM 9 at 1000 and 2320 m depth during LION1 (September 2007/March 2008) and one Aanderaa RCM 9 at 1000m LION2 (September 2008). Hence, during these two first deployments, we solely get the horizontal currents from the current meters. The vertical resolution was improved during LION3 and since then, with 20 potential temperature records, 10 salinity records, and 5 current records spanning depths from 150 to 2320 m (30 m above the seabed). Here, the Aquadopp temperature data were not used because of the low resolution and accuracy of the sensor (0.1°) and much more accurate temperature data were available from other sensors at about the same depths (several meters).

The severe environmental conditions imposed the use of a subsurface mooring, although the record of the upper 150 m heat content was prevented. However, surface data could be obtained by glider profiles

crossing nearby (<30 km) and by temperature records of the MF-LION meteorological buoy situated at <4.5 km from the deep mooring (see section 2.2). RBR 1050/1060 and SBE56 temperature recorders were set up with a 15 s sampling, while SBE37 CTD recorders and current meters had a sampling of 6 and 30 min, respectively. In order to have a consistent data set with 30 min sampling rate, we subsampled the time series recorded at a higher frequency.

The recovery percentage was satisfactory both for current meters (93%), temperature sensors (93%), and CTD sensors (96%). In particular, due to a breaking at the base of the line during the recovery (April 2009), we lost the bottom Aquadopp and no current data were obtained at 2300 m for the period from September 2008 to March 2009. During LION5, there were some battery issues on five SBE37 CTDs (165, 1100, 1300, 1780, and 200 m) that stopped recording in February 2011. A delayed recovery of the mooring in July 2012 caused battery issues for most of the current meters: the 150 m and the 2320 m current meters stopped recording on 11 June 2012, while the 250 m and the 500 m depth stopped on 14 July 2012.

Since the recovery of LION4 (in June 2010), intercalibration of the moored instruments, after and before each deployment, is performed. Niskin bottles are removed from the shipboard Rosette, and then Microcat and RBR (or SBE56) are attached instead. We perform a hydrographic cast with a 20 min stop at 1000 m depth, thus we can have a relative calibration of the moored instruments with the CTD probe SBE911plus. Post and/or precruise calibrations, together with in-laboratory analysis of salinity bottles with a Salinometer (Guildline Autosol) calibrated using standard water, provide an absolute accuracy of the measurements. Overall, for all deep mooring data used in this study, calibration error was lower than 0.005 for S, and 0.001°C for θ . No intercalibration was done from September 2007 to April 2009. At that time, comparisons with CTD stations were the only solution to detect possible biases in the conductivity measurements. In this

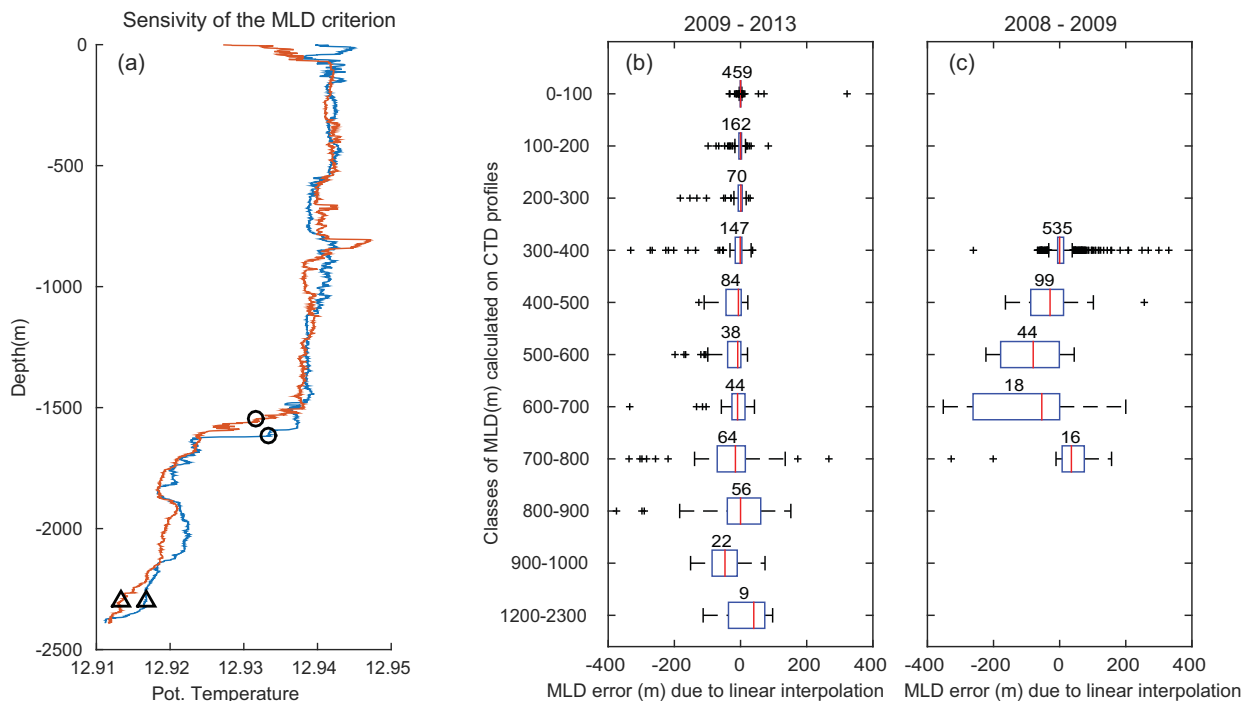


Figure B1. (a) Potential temperature profiles from 4 March 2011 carried out during the CASCADE cruise. The black triangles show the MLD calculated using a $\Delta\theta = 0.1^\circ\text{C}$ with a reference level at 10 m. The black circles show the MLD calculated using a double criterion: if the MLD, calculated using a $\Delta\theta_1 = 0.1^\circ\text{C}$ criterion with a reference level at 10 m, is deeper than 300 m, the MLD is defined by a second criterion: $\Delta\theta_2 = 0.01^\circ\text{C}$ with a reference level at 300 m. The MLD errors due to the depth resolution of the mooring are estimated by using CTD profiles (from research vessels, gliders, and profiling floats): (b) for the depth resolution of the mooring after 2009, and (c) for the period before the deployment of the thermistor chain below the MF-LION buoy in 2009. The MLD is calculated using the double potential temperature criterion defined in section 3.1. For each profile, the MLD error is calculated as the difference between the MLD calculated on a 1 m-bin averaged profile and the MLD calculated on the same profile, but subsampled at the mooring levels and linearly interpolated. The distribution of errors is binned in different MLD classes and is plotted as box plots. The number of samples used for each MLD class is indicated by the italic number on top of each box. The left side and right side of each blue “box” are the 25th and 75th percentiles of the samples, respectively. The distances between the left and right of the box are the interquartile ranges. The red line in the middle of each box is the sample median. The black lines extending from the left and right of each box are drawn from the left or right of the box to the furthest observations within 1.5 times the interquartile range. Outliers are displayed as black crosses.

study, the conductivity corrections applied to the SBE37 CTD correspond to equivalent salinity corrections ranging from 0.000 to 0.005 (details in *Houpert* [2014]).

Appendix B: Mixed Layer Depth Calculation

We choose a criterion $\Delta\theta_1$ large enough to overcome the lower accuracy of the sensors attached below the surface buoy. From November 2009 to July 2013, we choose $\Delta\theta_1 = 0.1^\circ\text{C}$ and a reference level at 10 m. Compared to the commonly used $\Delta\theta = 0.2^\circ\text{C}$ criterion [*De Boyer Montegut et al.*, 2004; *D'Ortenzio et al.*, 2005], this 0.1°C criterion reduces the difference between a MLD calculated with a potential temperature criterion and a MLD calculated on potential temperature-salinity profiles with an equivalent density criterion [*Houpert et al.*, 2015]. Using this first criterion, a Mixed Layer Depth (MLD) was calculated for the first 300 m of the upper water column.

A second criterion was required to define a more accurate MLD from the deep mooring data, as potential temperature gradients at the base of the ML can be smaller than $d\theta = 0.1^\circ\text{C}$ in winter when the mixing exceed 1000 m depth (Figure B1a). A $\Delta\theta_1 = 0.1^\circ\text{C}$ is better adapted for the surface layer where the vertical gradient is stronger. For the deep layers, the criterion has to be small enough to distinguish the homogenized mixed layer from the underlying deep waters. After performing sensibility tests for different potential temperature criteria and regarding the accuracy of the temperature sensors used on the LION mooring, we defined a $\Delta\theta_2 = 0.01^\circ\text{C}$ criterion and a reference level at 300 m, corresponding to the depth of the first SBE37 CTD of the deep LION mooring located below the LION buoy oceanographic sensors. If the MLD calculated with the $\Delta\theta_1$ criterion was deeper than 300m, then we used the second criterion $\Delta\theta_2$ to define the MLD, otherwise the MLD is calculated only with the $\Delta\theta_1$ criterion.

Since there was no instrument below the MF-LION surface buoy before November 2009, we could only use the sea surface temperature sensor at 1 m depth for the winter 2007–2008 and 2008–2009. Due to the low accuracy of this sensor and the diurnal variability, we tested different criteria. We select the smallest $\Delta\theta$ criterion that indicates the periods where the MLD reached 300 m depth in agreement with the potential temperature time series of the top of the LION mooring (150, 200, 230, 250, 300 m depth, more details in Table 1). We choose a criterion of 0.6°C calculated between the potential temperature at 1 m and the potential temperature at 300 m: if the potential temperature difference between 1m and 300 m is below 0.6°C , as for the 2009–2013 period, the MLD is defined by a second criterion $\Delta\theta_2 = 0.01^\circ\text{C}$ and a reference level at 300 m depth.

The potential temperature profiles used for the calculation of the MLD were linearly interpolated between the different mooring levels. We estimate the errors associated with the linear interpolation of the potential temperature profiles by using all the available CTD profiles from 2007 to 2013 (ship CTD, gliders, profiling floats) and by calculating for each profile the difference between the MLD calculated on the high-resolution CTD profile and the MLD calculated on the same profile subsampled at the mooring vertical resolution and linearly interpolated (Figure B1b and B1c). The improvements in the estimation on the MLD after the installation of the thermistor chain below the MF-LION buoy can be seen in Figure B1b. After 2009, the errors on the MLD are about $O(1\text{ m})$ in the first 100 m, $O(10\text{ m})$ from 100 to 400 m depth and $O(50\text{ m})$ below 400 m depth.

Appendix C: A 1-D Model to Study the Role of Winter Buoyancy Losses and Hydrographic Preconditioning

Following *Mertens and Schott* [1998], we can express the surface buoyancy flux B , which depends on the heat and freshwater fluxes at the sea surface, as:

$$B = \frac{g}{\rho_0} \left(\frac{\alpha_\theta}{c_w} Q_{\text{net}} + \rho_0 \beta_S S (E - P) \right) \quad (\text{C1})$$

where $g = 9.81\text{ m.s}^{-2}$ is the acceleration due to gravity, $\rho_0 = 1000\text{ kg.m}^{-3}$ is the density reference, $\alpha_\theta = 2 \times 10^{-4}\text{ .K}^{-1}$ and $\beta_S = 7.6 \times 10^{-4}$ are the thermal expansion and haline contraction coefficients, $c_w = 4000\text{ J.K.g}^{-1}\text{ .K}^{-1}$ is the heat capacity of water, Q_{net} is the surface net heat loss, S is the sea surface salinity, and $E - P$ represents the net freshwater flux.

The buoyancy content (BC) of the water column is defined as:

$$BC(t) = \frac{g}{\rho_0} \int \rho(z, t) dz \quad (C2)$$

The conservation of the BC undergoing a buoyancy flux $B(t)$ between t and $t + dt$ implies:

$$BC(t+dt) - BC(t) = \int B(t) dz \quad (C3)$$

Following Turner's formalism [Turner, 1973] and hypothesis (i.e., the vertical mixing is nonpenetrative) proposed by [Lascazatos and Nittis, 1998], the buoyancy flux required to mix an initially stratified water column down to the depth h can be written as:

$$\frac{h \partial h}{\partial t} = \frac{B(t)}{N^2(h)} \quad (C4)$$

where N is the buoyancy frequency ($N^2 = -\frac{g}{\rho_0} \frac{\partial \rho}{\partial z}$), and $B(t)$ the surface buoyancy flux defined in equation (C1).

Integrating equation (C4) gives:

$$IS(Z) = \int_0^Z h N^2(h) dh = \int_{t_0}^{t_1} B(t) dt \quad (C5)$$

where $IS(Z)$ represents an index of stratification of the water column [Herrmann et al., 2010].

In this work, we calculated $IS(Z)$ using the interpolated mooring and buoy data (see section 3.2) and we evaluated the possible source of errors. Before November 2011, the stratification due to the salinity in the first 200 m is unknown because of the absence of a conductivity sensor at the sea surface. To tackle this problem, we used then a constant value corresponding to the shallowest salinity measurement (at 170 m depth). To evaluate the error due to this approximation, we calculate $IS(Z)$ using high-resolution potential temperature and salinity profiles collected in a 30 km radius from the mooring (from gliders, and research vessels). Then, we compared $IS(Z)$ to $IS_{50}(Z)$, calculated with a constant salinity in the upper ocean. We also estimated the error due to the low vertical resolution by computing IS_{50} using the same salinity and potential temperature profiles but subsampled at the depth of the sensors on the mooring (similar to the method presented in section 3.2).

Another potential source of error can come from biases in vertical density gradients induced by the intercalibration of the different instruments. As we estimated an error in the calculation of the potential density less than 0.005 kg m^{-3} (due essentially to the calibration of the conductivity sensors), we propagated this error in the calculation of IS . For an integration to 1000 m depth, the error due to the accuracy of the intercalibration of the instruments represents between 13% and 34% of the total error (shown in section 4.2.4). If we use a stratification index integrated down to 2300 m, the errors due to the intercalibration of the instruments become too large (76%–92% of the total error) to have a relevant use of a stratification index calculated using the mooring. The winter convection can be considered deep when it penetrates deeper than the LIW (the intermediate water mass, located around 400 m depth) in the Northwestern Mediterranean Sea, so a stratification index $IS(1000)$ integrated down to 1000 m depth is enough to identify deep convection event.

References

- Artale, V., D. Iudicone, R. Santoleri, V. Rupolo, and S. Marullo (2002), Role of surface fluxes in ocean general circulation models using satellite sea surface temperature: Validation of and sensitivity to the forcing frequency of the Mediterranean thermohaline circulation, *J. Geophys. Res.*, 107(C8), 3120, doi:10.1029/2000JC000452.
- Bethoux, J. P., B. Gentili, J. Raunet, and D. Tailliez (1990), Warming trend in the western Mediterranean deep water, *Nature*, 347(6294), 660–662, doi:10.1038/347660a0.
- Bethoux, J. P., B. Gentili, D. Tailliez, and J. Bethoux (1998), Warming and freshwater budget change in the Mediterranean since the 1940 s, their possible relation to the greenhouse effect, *Geophys. Res. Lett.*, 25(7), 1023–1026, doi:10.1029/98GL00724.
- Bethoux, J. P., X. Durieu de Madron, F. Nyffeler, and D. Tailliez (2002), Deep water in the western Mediterranean: Peculiar 1999 and 2000 characteristics, shelf formation hypothesis, variability since 1970 and geochemical inferences, *J. Mar. Syst.*, 33–34, 117–131, doi:10.1016/S0924-7963(02)00055-6.
- Bosse, A, P. Testor, G. Legland, L. Mortier, L. Houpert, and L. Prieur (2014), Vertical velocities associated with open-ocean deep convection in the northwestern Mediterranean Sea as indirectly observed by gliders, Abstracts EGU2014–16009 presented at EGU General Assembly Conference, EGU. [Available at <http://www.eposters.net/pdfs/vertical-velocities-associated-with-deep-open-ocean-convection-in-the-northwestern-mediterranean.pdf>].

Acknowledgments

This study acknowledges the support of the MOOSE observation network of the northwestern Mediterranean, the HERMIONE (FP7-ENV-2008-1-226354) and PERSEUS (FP7-OCEAN.2011-3-287600) projects funded by the European Union under FP7, and the French "Equipement d'avenir" NAOS project (ANR J11R107-F). It is a contribution to the MerMex and HyMeX projects of the MISTRALS program. The authors would like to acknowledge the captains and crew members of R/V *Le Tethys II*, R/V *L'Atlante*, and R/V *Le Suroit*; the staff of the DT-INSU national pool of gliders; and all the scientists and support scientists who participated in the different research cruises and in the maintenance of the moored instruments. The authors would like to thank Harry Bryden, Vassilis P. Papadopoulos, and two anonymous reviewers for their precious comments which greatly improve the quality of the manuscript. We would like also to thank Matthew Toberman for helping us to improve the language of this manuscript. The data used are listed in the data section. The MODIS Aqua surface chlorophyll concentration data can be obtained from the NASA web site (<http://oceancolor.gsfc.nasa.gov/>). Cruises, floats, and gliders data can be accessed from the Coriolis Data Center (<http://www.coriolis.eu.org/>). The LION mooring data can be accessed through the SEANOE (SEA scieNtific Open data Edition) portal, operated by Sismer: doi:10.17882/44411. The MF-LION buoy data were obtained from the HyMeX program, sponsored by grants MISTRALS/HyMeX and Météo-France; SST, SSS, and 0–250 m ocean temperature data be downloaded from <http://data.datacite.org/10.6096/HyMeX.LionBuoy.Thermosalinograph.20100308>; <http://data.datacite.org/10.6096/MISTRALS-HyMeX-MOOSE.1025>; and <http://data.datacite.org/10.6096/MISTRALS-HyMeX-MOOSE.388>. We acknowledge the CMM (Météo-France) for installing and maintaining the MF-LION buoy and corresponding sensors.

- Bosse, A., P. Testor, L. Mortier, L. Prieur, V. Taillandier, F. d'Ortenzio, and L. Coppola (2015), Spreading of Levantine intermediate waters by submesoscale coherent vortices in the northwestern Mediterranean Sea as observed with gliders, *J. Geophys. Res. Oceans*, *120*, 1599–1622, doi:10.1002/2014JC010263.
- Bosse, A., et al. (2016), Scales and dynamics of submesoscale coherent vortices formed by deep convection in the northwestern Mediterranean Sea, *J. Geophys. Res. Oceans*, doi:10.1002/2016JC012144, in press.
- Bryden, H. L., J. Candela, and T. H. Kinder (1994), Exchange through the Strait of Gibraltar, *Prog. Oceanogr.*, *33*(3), 201–248, doi:10.1016/0079-6611(94)90028-0.
- Canals, M., P. Puig, X. D. de Madron, S. Heussner, A. Palanques, and J. Fabres (2006), Flushing submarine canyons, *Nature*, *444*(7117), 354–357, doi:10.1038/nature05271.
- Candela, J. (2001), Chapter 5.7 Mediterranean water and global circulation, in *International Geophysics*, edited by G. Siedler, J. Church, and J. Gould, vol. 77, pp. 419–429, Academic Press, doi:10.1016/S0074-6142(01)80132-7.
- CIESM (2009), Dynamics of Mediterranean Deep Waters, *CIESM Work Monogr.*, *38*, 132 p.
- Clarke, R. A., and J.-C. Gascard (1983), The formation of Labrador Sea water. Part I: Large-scale processes, *J. Phys. Oceanogr.*, *13*(10), 1764–1778, doi:10.1175/1520-0485(1983)013<1764:TFOLSW>2.0.CO;2.
- De Boyer Montegut, C., Madec, G., Fischer, A. S. Fischer, and D. Iudicone (2004), Mixed layer depth over the global ocean: An examination of profile data and a profile based climatology, *J. Geophys. Res.*, *109*, C12003, doi:10.1029/2004JC002378.
- Dee, D. P., et al. (2011), The ERA-Interim reanalysis: Configuration and performance of the data assimilation system, *Q. J. R. Meteorol. Soc.*, *137*, 553–597, doi:10.1002/qj.828.
- De Jong, M. F., A. S. Bower, and H. H. Furey (2014), Two years of observations of warm-core anticyclones in the Labrador Sea and their seasonal cycle in heat and salt stratification, *J. Phys. Oceanogr.*, *44*(2), 427–444, doi:10.1175/JPO-D-13-070.1.
- D'Ortenzio, F., D. Iudicone, C. De Boyer Montegut, P. Testor, D. Antoine, S. Marullo, R. Santoleri, and G. Madec (2005), Seasonal variability of the mixed layer depth in the Mediterranean Sea as derived from in situ profiles, *Geophys. Res. Lett.*, *32*, L12605, doi:10.1029/2005GL022463.
- Drobinski, P., et al. (2014) HyMeX: A 10-year multidisciplinary program on the Mediterranean water cycle, *Bull. Am. Meteorol. Soc.*, *95*, 1063–1082, doi:10.1175/BAMS-D-12-00242.1.
- Durrieu de Madron, X., et al. (2013), Interaction of dense shelf water cascading and open-sea convection in the northwestern Mediterranean during winter 2012, *Geophys. Res. Lett.*, *40*, 1379–1385, doi:10.1002/grl.50331.
- Fan, X., U. Send, P. Testor, J. Karstensen, and P. Lherminier (2013), Observations of Irminger Sea anticyclonic eddies, *J. Phys. Oceanogr.*, *43*(4), 805–823, doi:10.1175/JPO-D-11-0155.1.
- Font, J., P. Puig, J. Salat, A. Palanques, and M. Emelianov (2007), Sequence of hydrographic changes in NW Mediterranean deep water due to the exceptional winter of 2005, *Sci. Mar.*, *71*(2), 339–346, doi:10.3989/scimar.2007.71n2339.
- Frajka-Williams, E., C. C. Eriksen, P. B. Rhines, and R. R. Harcourt (2011), Determining vertical water velocities from Seaglider, *J. Atmos. Oceanic Technol.*, *28*(12), 1641–1656, doi:10.1175/2011JTECH0830.1.
- Gasparini, G. P., A. Ortona, G. Budillon, M. Astraldi, and E. Sansone (2005), The effect of the Eastern Mediterranean Transient on the hydrographic characteristics in the Strait of Sicily and in the Tyrrhenian Sea, *Deep Sea Res., Part I*, *52*(6), 915–935, doi:10.1016/j.dsr.2005.01.001.
- Grignon, L. (2009), *Causes of the Interannual Variability of Deep Convection*, Univ. of Southampton. [Available at <http://eprints.soton.ac.uk/72147/>]
- Grignon, L., D. A. Smeed, H. L. Bryden, and K. Schroeder (2010), Importance of the variability of hydrographic preconditioning for deep convection in the Gulf of Lion, NW Mediterranean, *Ocean Sci.*, *6*(2), 573–586, doi:10.5194/os-6-573-2010.
- Hátún, H., C. C. Eriksen, and P. B. Rhines (2007), Buoyant eddies entering the Labrador Sea observed with gliders and altimetry, *J. Phys. Oceanogr.*, *37*(12), 2838–2854, doi:10.1175/2007JPO3567.1.
- Herrmann, M., S. Somot, F. Sevault, C. Estournel, and M. Déqué (2008), Modeling the deep convection in the northwestern Mediterranean Sea using an eddy-permitting and an eddy-resolving model: Case study of winter 1986–1987, *J. Geophys. Res.*, *113*, C04011, doi:10.1029/2006JC003991.
- Herrmann, M., F. Sevault, J. Beuvier, and S. Somot (2010), What induced the exceptional 2005 convection event in the northwestern Mediterranean basin? Answers from a modeling study, *J. Geophys. Res.*, *115*, C12051, doi:10.1029/2010JC006162.
- Herrmann, M., S. Somot, S. Calmanti, C. Dubois, and F. Sevault (2011), Representation of daily wind speed spatial and temporal variability and intense wind events over the Mediterranean Sea using dynamical downscaling: Impact of the regional climate model configuration, *Nat. Hazards Earth Syst. Sci.*, *11*, 1983–2001, doi:10.5194/nhess-11-1983-2011.
- Houpert, L. (2013), Contribution to the Study of Transfer Processes from the Surface to the Deep Ocean in the Mediterranean Sea Using in-situ Measurements, PhD thesis, Université de Perpignan Via Domitia. [Available at <https://tel.archives-ouvertes.fr/tel-01148986>]
- Houpert, L. (2014), Technical report on the intercalibration of the sensors on the LION mooring line, LOCEAN, Univ. Pierre et Marie Curie, Paris, 19 pp. [Available at http://lhoupert.fr/files/report/2014_intercalib_sensors_LION.pdf]
- Houpert L., P. Testor, X. Durrieu de Madron, S. Somot, F. D'Ortenzio, C. Estournel, and H. Lavigne (2015), Seasonal cycle of the mixed layer, the seasonal thermocline and the upper-ocean heat storage rate in the Mediterranean Sea derived from observations, *Prog. Oceanogr.*, *132*, 333–352, doi:10.1016/j.pocean.2014.11.004.
- Josey, S. A., S. Somot, and M. Tsimplis (2011), Impacts of atmospheric modes of variability on Mediterranean Sea surface heat exchange, *J. Geophys. Res.*, *116*, C02032, doi:10.1029/2010JC006685.
- Juza, M., L. Renault, S. Ruiz, and J. Tintoré (2013), Origin and pathways of Winter Intermediate Water in the Northwestern Mediterranean Sea using observations and numerical simulation, *J. Geophys. Res. Oceans*, *118*, 6621–6633, doi:10.1002/2013JC009231.
- Killworth, P. D. (1983), Deep convection in the World Ocean, *Rev. Geophys.*, *21*(1), 1–26, doi:10.1029/RG021i001p00001.
- Kim, K., K.-I. Chang, D.-J. Kang, Y., Y. H. Kim, and J.-H. Lee (2008), Review of recent findings on the water masses and circulation in the East Sea (Sea of Japan), *J. Oceanogr.*, *64*(5), 721–735, doi:10.1007/s10872-008-0061-x.
- Klein, B., W. Roether, B. B. Manca, D. Bregant, V. Beitzel, V. Kovacevic, and A. Luchetta (1999), The large deep water transient in the Eastern Mediterranean, *Deep Sea Res., Part I*, *46*(3), 371–414, doi:10.1016/S0967-0637(98)00075-2.
- Krahmann, G., and F. Schott (1998), Long-term increases in western Mediterranean salinities and temperatures: Anthropogenic and climatic sources, *Geophys. Res. Lett.*, *25*(22), 4209–4212, doi:10.1029/1998GL900143.
- Lacombe, H., P. Tchernia, and L. Gamberoni (1985), Variable bottom water in the Western Mediterranean basin, *Prog. Oceanogr.*, *14*(1971), 319–338, doi:10.1016/0079-6611(85)90015-1.
- Lascaratos, A., and K. Nittis (1998), A high-resolution three-dimensional numerical study of intermediate water formation in the Levantine Sea, *J. Geophys. Res.*, *103*(C9), 18,497–18,512.

- Lasarcatos, A., W. Roether, K. Nittis, and B. Klein (1999), Recent changes in deep water formation and spreading in the eastern Mediterranean Sea: A review, *Prog. Oceanogr.*, *44*(1–3), 5–36, doi:10.1016/S0079-6611(99)00019-1.
- Lavigne, H., F. D'Ortenzio, C. Migon, H. Claustre, P. Testor, M. Ribera d'Alcalà, R. Lavezza, L. Houpert, and L. Prieur (2013), Enhancing the comprehension of mixed layer depth control on the Mediterranean phytoplankton phenology, *J. Geophys. Res. Oceans*, *118*, 3416–3430, doi:10.1002/jgrc.20251.
- Lazier, J. R. N. (1973), The renewal of Labrador sea water, *Deep Sea Res., Oceanogr. Abstr.*, *20*(4), 341–353, doi:10.1016/0011-7471(73)90058-2.
- Leaman, K. D., and F. A. Schott (1991), Hydrographic structure of the convection regime in the Gulf of Lions: Winter 1987, *J. Phys. Oceanogr.*, *21*(4), 575–598, doi:10.1175/1520-0485(1991)021<0575:HSOTCR>2.0.CO;2.
- Legg, S., and J. C. McWilliams (2001), Convective modifications of a geostrophic eddy field, *J. Phys. Oceanogr.*, *31*(4), 874–891, doi:10.1175/1520-0485(2001)031<0874:CMOAGE>2.0.CO;2.
- Lherminier, P., J.-C. Gascard, and D. Quadfasel (1999), The Greenland Sea in Water 1993 and 1994: Preconditioning for deep convection, *Deep Sea Res., Part II*, *46*(6–7), 1199–1235, doi:10.1016/S0967-0645(99)00020-X.
- L'Hévéder, B., L. Li, F. Sevault, and S. Somot (2013), Interannual variability of deep convection in the Northwestern Mediterranean simulated with a coupled AORCM, *Clim. Dyn.*, *41*(3), 937–960, doi:10.1007/s00382-012-1527-5.
- Lilly, J. M., and P. B. Rhines (2002), Coherent eddies in the Labrador Sea observed from a mooring, *J. Phys. Oceanogr.*, *32*(2), 585–598, doi:10.1175/1520-0485(2002)032<0585:CEITLS>2.0.CO;2.
- Lilly, J. M., P. B. Rhines, M. Visbeck, R. Davis, J. R. N. Lazier, F. Schott, and D. Farmer (1999), Observing deep convection in the Labrador Sea during Winter 1994/95, *J. Phys. Oceanogr.*, *29*(8), 2065–2098, doi:10.1175/1520-0485(1999)029<2065:ODCITL>2.0.CO;2.
- Lilly, J. M., P. B. Rhines, F. Schott, K. Lavender, J. Lazier, U. Send, and E. D'Asaro (2003), Observations of the Labrador Sea eddy field, *Prog. Oceanogr.*, *59*(1), 75–176, doi:10.1016/j.pocean.2003.08.013.
- López-Jurado, J.-L., C. González-Pola, and P. Vélez-Belchí (2005), Observation of an abrupt disruption of the long-term warming trend at the Balearic Sea, western Mediterranean Sea, in summer 2005, *Geophys. Res. Lett.*, *32*, L24606, doi:10.1029/2005GL024430.
- Malanotte-Rizzoli, P., B. B. Manca, M. R. D'Alcala, A. Theocharis, S. Brenner, G. Budillon (1999), The Eastern Mediterranean in the 80s and in the 90s: The big transition in the intermediate and deep circulations, *Dyn. Atmos. Oceans*, *29*(2–4), 365–395, doi:10.1016/S0377-0265(99)00011-1.
- Marshall, J., and F. Schott (1999), Open-ocean convection: Observations, theory, and models, *Rev. Geophys.*, *37*(1), 1–64, doi:10.1029/98RG02739.
- McWilliams, J. C. (1985), Submesoscale, coherent vortices in the ocean, *Rev. Geophys.*, *23*(2), 165–182, doi:10.1029/RG023i002p00165.
- MEDOC Group (1970), Observation of formation of deep water in the Mediterranean Sea, 1969, *Nature*, *227*(5262), 1037–1040, doi:10.1038/2271037a0.
- Merkelbach, L., D. Smeed, and G. Griffiths (2010), Vertical water velocities from underwater gliders, *J. Atmos. Oceanic Technol.*, *27*(3), 547–563, doi:10.1175/2009JTECHO710.1.
- Mermex Group (2011), Marine ecosystems responses to climatic and anthropogenic forcings in the Mediterranean, *Prog. Oceanogr.*, *91*(2), 97–166, doi:10.1016/j.pocean.2011.02.003.
- Mertens, C., and F. Schott (1998), Interannual variability of deep-water formation in the Northwestern Mediterranean, *J. Phys. Oceanogr.*, *28*(7), 1410–1424, doi:10.1175/1520-0485(1998)028<1410:IVODWF>2.0.CO;2.
- Millot, C. (1999), Circulation in the western Mediterranean Sea, *J. Mar. Syst.*, *20*(1–4), 423–442, doi:10.1016/S0924-7963(98)00078-5.
- Millot, C. (2007), Interannual salinification of the Mediterranean inflow, *Geophys. Res. Lett.*, *34*, L21609, doi:10.1029/2007GL031179.
- Puig, P., A. Palanques, and J. Martín (2013a), Contemporary sediment-transport processes in submarine canyons, *Annu. Rev. Mar. Sci.*, *6*, 53–77, doi:10.1146/annurev-marine-010213-135037.
- Puig, P., et al. (2013b), Thick bottom nepheloid layers in the western Mediterranean generated by deep dense shelf water cascading, *Prog. Oceanogr.*, *111*, 1–23, doi:10.1016/j.pocean.2012.10.003.
- Rixen, M. et al. (2005), The western Mediterranean deep water: A proxy for climate change, *Geophys. Res. Lett.*, *32*, L12608, doi:10.1029/2005GL022702.
- Rohling, E. J., and H. L. Bryden (1992), Man-induced salinity and temperature increases in western Mediterranean deep water, *J. Geophys. Res.*, *97*(C7), 11,191–11,198, doi:10.1029/92JC00767.
- Salat, J., M. Emelianov, and J. L. López-Jurado (2006), Unusual extension of Western Mediterranean deep water formation during winter 2005, in *Proceedings of 5th Asamblea Hispano-Portuguesa de Geodesia y Geofísica*, Univ. Sevilla, Sevilla, Spain.
- Schott, F., and K. D. Leaman (1991), Observations with moored acoustic doppler current profilers in the convection regime in the Golfe du Lion, *J. Phys. Oceanogr.*, *21*(4), 558–574, doi:10.1175/1520-0485(1991)021<0558:OWMADC>2.0.CO;2.
- Schott, F., M. Visbeck, and J. Fischer (1993), Observations of vertical currents and convection in the central Greenland Sea during the winter of 1988–1989, *J. Geophys. Res.*, *98*(C8), 14,401–14,421, doi:10.1029/93JC00658.
- Schott, F., M. Visbeck, U. Send, J. Fischer, L. Stramma, and Y. Desaubies (1996), Observations of deep convection in the Gulf of Lions, Northern Mediterranean, during the Winter of 1991/92, *J. Phys. Oceanogr.*, *26*(4), 505–524, doi:10.1175/1520-0485(1996)026<0505:OOD-CIT>2.0.CO;2.
- Schroeder, K., G. P. Gasparini, M. Tangherlini, and M. Astraldi (2006), Deep and intermediate water in the western Mediterranean under the influence of the Eastern Mediterranean Transient, *Geophys. Res. Lett.*, *33*, L21607, doi:10.1029/2006GL027121.
- Schroeder, K., A. Ribotti, M. Borghini, M. Sorgente, R. Perilli, and A. Gasparini (2008a), An extensive western Mediterranean deep water renewal between 2004 and 2006, *Geophys. Res. Lett.*, *35*, L18605, doi:10.1029/2008GL035146.
- Schroeder, K., V. Taillandier, A. Vetrano, and G. P. Gasparini (2008b), The circulation of the western Mediterranean Sea in spring 2005 as inferred from observations and from model outputs, *Deep Sea Res., Part I*, *55*(8), 947–965, doi:10.1016/j.dsr.2008.04.003.
- Schroeder, K., S. A. Josey, M. Herrmann, L. Grignon, G. P. Gasparini, and H. L. Bryden (2010), Abrupt warming and salting of the Western Mediterranean Deep Water after 2005: Atmospheric forcings and lateral advection, *J. Geophys. Res.*, *115*, C08029, doi:10.1029/2009JC005749.
- Schroeder, K., et al. (2013), Long-term monitoring programme of the hydrological variability in the Mediterranean Sea: A first overview of the HYDROCHANGES network, *Ocean Sci.*, *9*(2), 301–324, doi:10.5194/os-9-301-2013.
- Send, U., and J. Marshall (1995), Integral effects of deep convection, *J. Phys. Oceanogr.*, *25*(5), 855–872.
- Severin, T., P. Conan, X. Durrieu de Madron, L. Houpert, M. J. Oliver, L. Oriol, J. Caparros, J. F. Ghigliani, and M. Pujo-Pay (2014), Impact of open-ocean convection on nutrients, phytoplankton biomass and activity, *Deep Sea Res., Part I*, *94*, 62–71.
- Smith, R. O., H. L. Bryden, and K. Stansfield (2008), Observations of new western Mediterranean deep water formation using Argo floats 2004–2006, *Ocean Sci.*, *4*(2), 133–149, doi:10.5194/os-4-133-2008.
- Somot, S., et al. (2016), Characterizing, modelling, and understanding the climate variability of the deep water formation in the North-Western Mediterranean Sea, *Clim. Dyn.*, 1–32, doi:10.1007/s00382-016-3295-0.

- Soto-Navarro, J., F. Criado-Aldeanueva, J. García-Lafuente, and A. Sánchez-Román (2010), Estimation of the Atlantic inflow through the Strait of Gibraltar from climatological and in situ data, *J. Geophys. Res.*, *115*, C10023, doi:10.1029/2010JC006302.
- Stabholz M., et al. (2013), Impact of open-sea convection on particulate fluxes and sediment dynamics in the deep basin of the Gulf of Lions, *Biogeosciences*, *10*, 1097–1116.
- Tamburini, C., et al. (2013), Deep-Sea bioluminescence blooms after dense water formation at the ocean surface, *PLoS ONE*, *8*(7), e67523, doi:10.1371/journal.pone.0067523.
- Testor, P., et al. (2007), European Gliding Observatories (EGO), *Coriolis Newsl.*, *4*, 11–12.
- Testor, P., et al. (2010), Gliders as a component of future observing systems, in *Proceedings of the "OceanObs'09: Sustained Ocean Observations and Information for Society,"* vol. 2, edited by J. Hall, D. E. Harrison, and D. Stammer, OceanObs'09, Venice, Italy.
- Testor, P., X. Durrieu De Madron, L. Mortier L., F. D'Ortenzio, H. Legoff, D. Dausse, M. Labaste, and L. Houpert (2016), LION observatory data, SEANOE, doi:10.17882/44411.
- THETIS Group (1994), Open-ocean deep convection explored in the Mediterranean, *Eos Trans. AGU*, *75*(19), 217–221, doi:10.1029/94EO00893.
- Tsimplis, M. and H. Bryden (2000), Estimation of the transports through the Strait of Gibraltar, *Deep Sea Res., Part I*, *47*(12), 2219–2242, doi:10.1016/S0967-0637(00)00024-8.
- Turner, J. (1973), *Buoyancy Effects in Fluids*, Cambridge Univ. Press. [Available at <http://dx.doi.org/10.1017/CBO9780511608827>.]
- Tziperman, E., and K. Speer (1994), A study of water mass transformation in the Mediterranean Sea: Analysis of climatological data and a simple three-box model, *Dyn. Atmos. Oceans*, *21*, 53–82.
- Vargas-Yanez, M., F. Moya, M. C. García-Martínez, E. Tel, P. Zunino, F. Plaza, J. Salat, J. Pascual, J. L. Lopez-Jurado, and M. Serra (2010a), Climate change in the western Mediterranean Sea 1900–2008, *J. Mar. Syst.*, *82*(3), 171–176, doi:10.1016/j.jmarsys.2010.04.013.
- Vargas-Yanez, M., P. Zunino, A. Benali, M. Delpy, F. Pastre, F. Moya, M. C. García-Martínez, and E. Tel (2010b), How much is the western Mediterranean really warming and salting?, *J. Geophys. Res.*, *115*, C04001, doi:10.1029/2009JC005816.
- Voorhis, A. D., and D. C. Webb (1970), Large vertical currents observed in a winter sinking region of the northwestern Mediterranean, *Cahiers Oceanogr.*, *XXII*(6), 571–580.
- Waldman, R., et al. (2016), Estimating dense water volume and its evolution for the year 2012–2013 in the North-western Mediterranean Sea: An observing system simulation experiment approach, *J. Geophys. Res.*, *121*, doi:10.1002/2016JC011694, in press.
- Zunino, P., K. Schroeder, M. Vargas-Yañez, G. P. Gasparini, L. Coppola, M. C. Garcia-Martinez, and F. Moya-Ruiz (2012), Effects of the Western Mediterranean Transition on the resident water masses: Pure warming, pure freshening and pure heaving, *J. Mar. Syst.*, *96–97*, 15–23.